nature structural & molecular biology

Article

https://doi.org/10.1038/s41594-024-01456-7

DARPin-induced reactivation of p53 in HPV-positive cells

Received: 1 February 2024

Accepted: 21 November 2024

Published online: 09 January 2025

Check for updates

Philipp Münick[1], Alexander Strubel[1], Dimitrios-Ilias Balourdas[2,3], Julianne S. Funk[4], Marco Mernberger[4], Christian Osterburg[1], Birgit Dreier[5], Jonas V. Schaefer[5], Marcel Tuppi[1], Büşra Yüksel[1,6], Birgit Schäfer[1], Stefan Knapp[2,3], Andreas Plückthun[5], Thorsten Stiewe[4,7,8], Andreas C. Joerger[2,3] & Volker Dötsch[1]

Infection of cells with high-risk strains of the human papillomavirus (HPV) causes cancer in various types of epithelial tissue. HPV infections are responsible for ~4.5% of all cancers worldwide. Tumorigenesis is based on the inactivation of key cellular control mechanisms by the viral proteins E6 and E7. The HPV E6 protein interacts with the cellular E3 ligase E6AP, and this complex binds to the p53 DNA-binding domain, which results in degradation of p53. Inhibition of this interaction has the potential to reactivate p53, thus preventing oncogenic transformation. Here we describe the characterization of a designed ankyrin repeat protein that binds to the same site as the HPV E6 protein, thereby displacing the E3 ligase and stabilizing p53. Interaction with the designed ankyrin repeat protein does not affect p53 DNA binding or the crucial MDM2 negative feedback loop but reactivates a p53-dependent transcriptional program in HeLa (HPV18-positive) and SiHa (HPV16-positive) cells, suggesting a potential therapeutic use.

Several subtypes of the human papillomavirus (HPV) cause anogenital carcinomas[1]. In particular, cervical cancer has been associated with HPV infection, with the two high-risk HPV16 and HPV18 subtypes being responsible for more than 70% of human cervical carcinoma, which rises to 90% when all HPV subtypes are included[2]. In addition to anogenital cancers, an HPV infection can also cause squamous cell carcinoma of the head and neck, in particular, squamous cell carcinoma of the head and neck located in the oral cavity (oropharyngeal squamous cell carcinoma)[3]. The molecular mechanism of the HPV-induced tumorigenesis is well studied and is based on the inactivation of important cellular factors by viral proteins, especially by the early expressed proteins E6 and E7 (refs. 4–7). Mechanistic investigations have revealed that the E7 protein binds to the tumor suppressor Rb and, thus, releases the transcription factor E2F1 (as well as E2F2 and E2F3)[8,9]. The second viral protein that is responsible for the transformation of cells is the E6 protein. It consists of two small Zn-binding domains that are flexibly linked by a helix[10,11], and it can bind leucine-rich peptides in the cleft between both domains[12]. One important interaction is the binding to the cellular E3 ligase E6AP. The E6AP leucine-rich peptide structures the cleft between both E6 domains and renders the complex capable of binding to the DNA-binding domain (DBD) of p53 (ref. 13). This interaction recruits the E6AP E3 ligase to the vicinity of p53, which results in ubiquitination and proteasomal degradation of p53 (ref. 14). Long-term infections with high-risk HPV viruses can, thus, transform cells[15,16]. The development of vaccination against high-risk HPV strains has become a powerful weapon against virus-induced tumorigenesis; however, vaccination is not available in many countries, especially developing countries where HPV-induced cancers continue to be a severe health problem. In addition to the expansion of vaccination programs, the development of an anti-HPV therapy would be important to provide

[1]Institute of Biophysical Chemistry and Center for Biomolecular Magnetic Resonance, Goethe University, Frankfurt, Germany. [2]Institute of Pharmaceutical Chemistry, Goethe University, Frankfurt, Germany. [3]Structural Genomics Consortium, Goethe University, Frankfurt, Germany. [4]Institute of Molecular Oncology, Universities of Giessen and Marburg Lung Center, Member of the German Center for Lung Research, Philipps-University, Marburg, Germany. [5]Department of Biochemistry, University of Zurich, Zurich, Switzerland. [6]IMPRS on Cellular Biophysics, Frankfurt, Germany. [7]Genomics Core Facility, Philipps-University, Marburg, Germany. [8]Institute for Lung Health, Justus Liebig University, Giessen, Germany. e-mail: vdoetsch@em.uni-frankfurt.de

https://doi.org/10.1038/s41594-024-01456-7

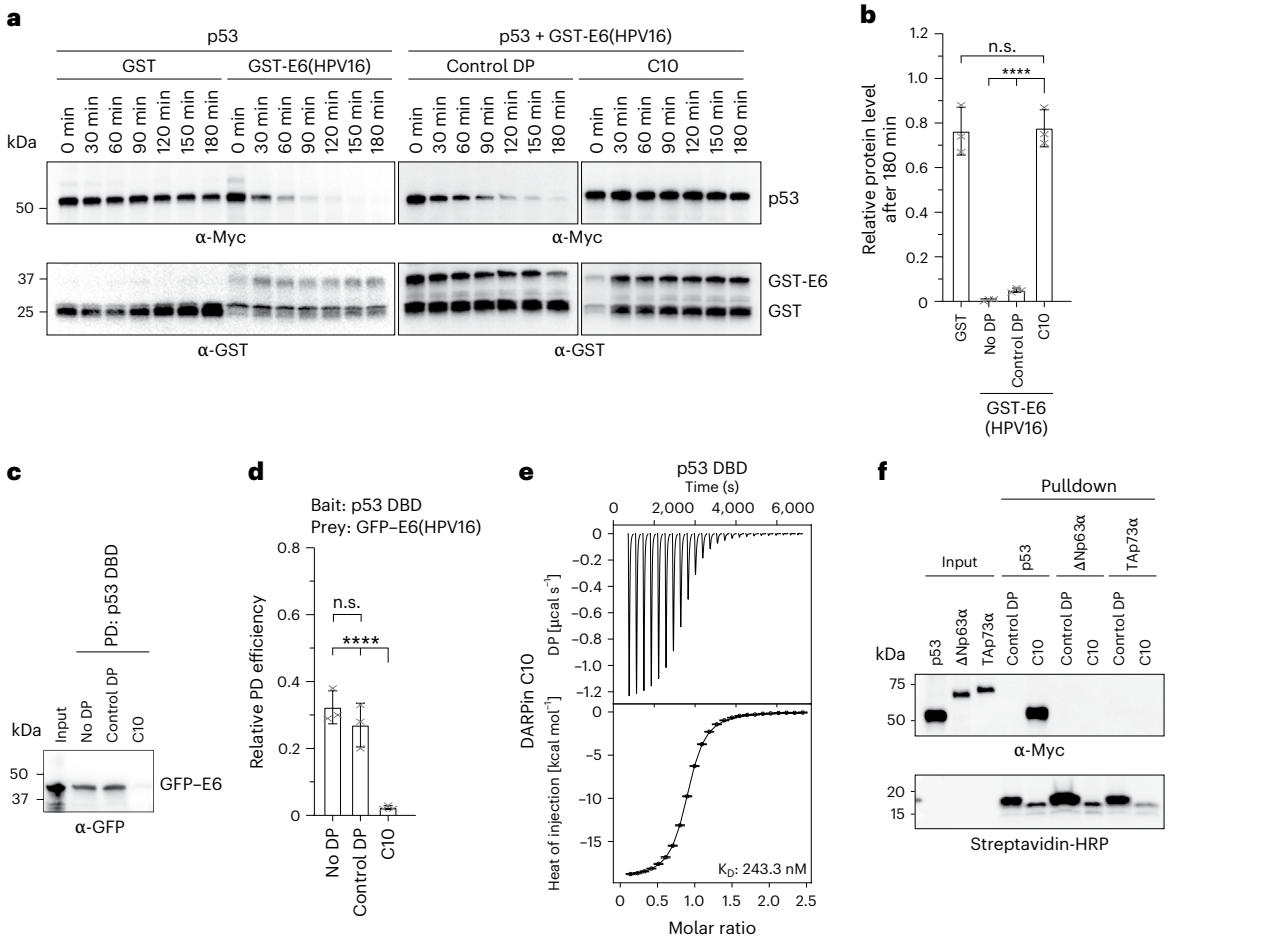

Fig. 1 | DARPin C10 inhibits the HPV-E6-mediated degradation of p53. a, Myc-tagged p53 was in vitro translated in RRLs and coincubated with a GST fusion of the HPV16-E6 protein, with or without the respective DARPin. Coincubation with GST did not show any degradation, whereas incubation with GST-E6 led to degradation of p53. Coincubation of p53 with E6 and DARPin C10 prevented degradation, while the control DARPin had no effect. **b**, A quantification of the degradation assay in **a**. The relative protein level after 180 min, normalized to the protein level after 0 min, is shown on the *y* axis. **c**, A pulldown of GFP-tagged E6 protein of HPV16 with immobilized p53 DBD and competition with DARPin C10. DARPin C10 efficiently blocked binding of E6 to the p53 DBD, while the control DARPin had no effect. **d**, Quantification of the pulldown experiment in **c**. The relative pulldown efficiency normalized to the input samples is shown on the *y* axis. **e**, An interaction study of the p53 DBD and DARPin C10 using ITC. The raw measurement (top) and the integrated heat per titration step (bottom) are shown. The K_d value for the interaction is given in the bottom right corner. The measurement was performed at 25 °C. The measurements were performed as technical duplicates with one being shown. The error bars represent the error of the fitting procedure. **f**, The pulldown experiments of p53 family members with DARPin C10 and a control DARPin. The H1299 cells were transiently transfected with Myc-tagged p53, ΔNp63α or TAp73α. The input signals are shown on the left and the pulldown signals on the right. The experiment was performed in biological triplicates, with one exemplary western blot shown. In **b** and **d**, the bar diagram shows the mean values and the error bars the corresponding s.d. of three biological replicates. An ordinary one-way ANOVA was performed to assess the statistical significance (n.s., $P > 0.05$; *$P \leq 0.05$, **$P \leq 0.01$, ***$P \leq 0.001$, ****$P \leq 0.0001$).

treatment options. One avenue toward such a therapy is the reactivation of p53 in HPV-infected cells. In principle, the cleft between the two Zn-binding domains of E6 could be druggable, and corresponding drug screens have already been performed[17]. A recent structure determination of a complex of full-length E6AP with HPV16 E6 has demonstrated that the interface between both proteins is large and not limited to the leucine-rich peptide, which explains the pM affinity between both proteins and the failure to target the E6–E6AP interaction therapeutically[18]. Nevertheless, inhibition of the degradation function of the E6 protein was demonstrated using a construct in which a leucine-rich peptide was fused to a PDZ domain[19]. This protein binds to both the cleft between the two Zn-binding domains and to the C-terminal peptide of E6 with nanomolar-scale affinity. In cell culture experiments, this bivalent ligand stabilized p53 and induced apoptosis in HPV-positive cells, although the inhibitory effect of the isolated PDZ domain was almost as strong as the one of the fusion construct[19].

An alternative to peptide-based reagents (which might not be stable in the intracellular environment) is designed ankyrin repeat proteins (DARPins)[20,21]. DARPins consist of multiple stacked helical hairpin units. Certain positions in the loops and in the helices are randomized to result in a contiguous interaction surface and can be used for in vitro selection of tight binders[20–23]. The advantages of DARPins relative to other selective binders such as antibodies are their small size (14–18 kDa), high stability and the absence of stabilizing disulfide bonds, which makes them ideally suited as inhibitors in the reducing cellular cytoplasm. Recently, we have developed DARPins against all folded domains of p63 (ref. 24) as well as DARPins that selectively target the heterotetramer consisting of a p63 dimer and a p73 dimer[25]. We have also developed DARPins that bind to the DBD of p53. While one of these DARPins binds to the DNA-binding surface and, thus, inhibits DNA binding and transcriptional activity[24], other DARPins targeted other regions of the p53 DBD. Intriguingly, the binding site of the E6 protein on the p53 DBD does not overlap with any known interaction interfaces, neither with DNA nor with proteins[13], including the important interactions between DBDs when cooperatively binding to DNA as a tetramer[26–28]. This opportunity exploited by the virus through

https://doi.org/10.1038/s41594-024-01456-7

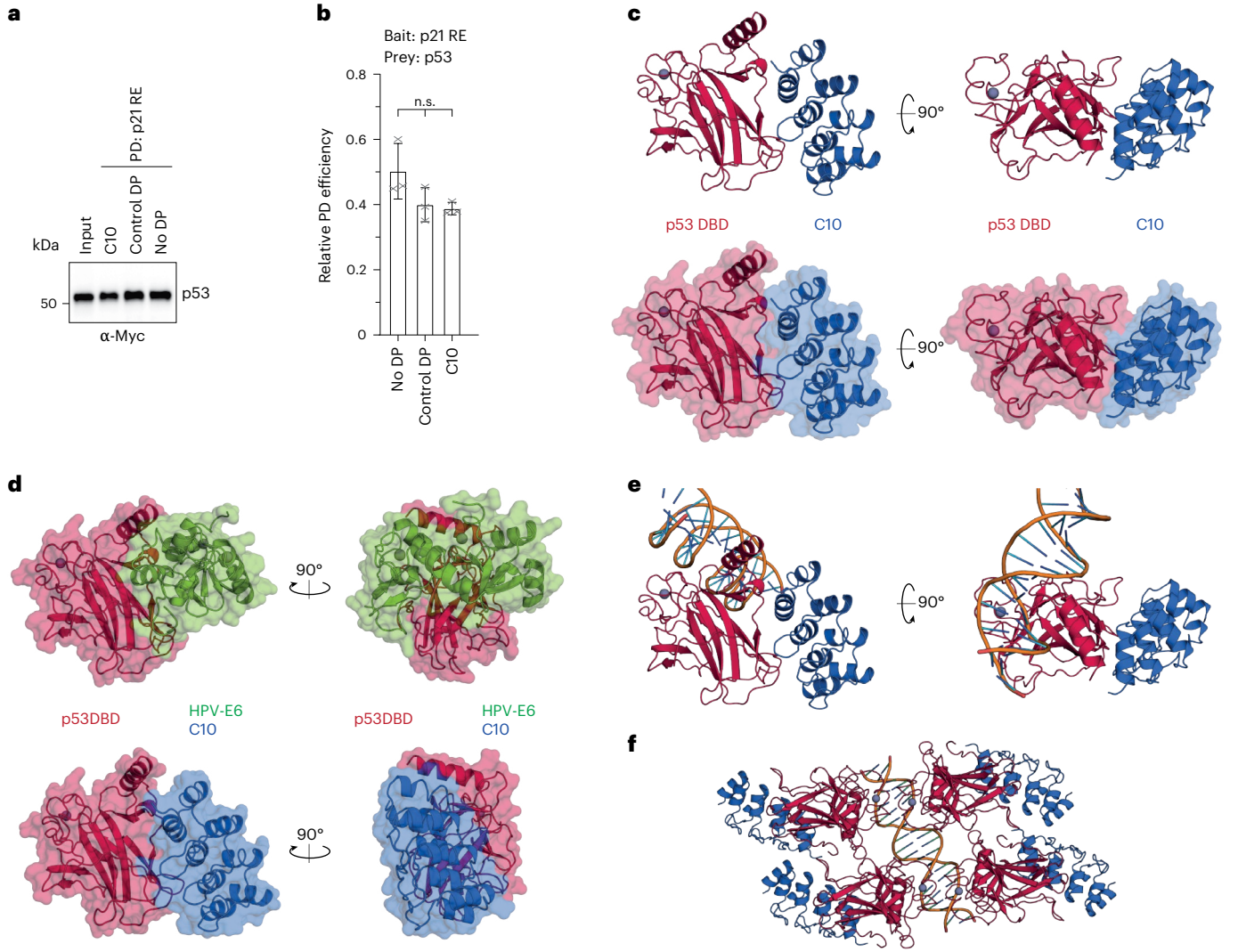

Fig. 2 | Investigation of the binding epitope of DARPin C10 on the p53 DBD. **a**, DNA pulldown experiments with p53 and an immobilized dsDNA oligomer containing the 20 bp binding site of the human p21 promotor (p21 RE). Preincubation of p53 with DARPin C10 or the control DARPin (DP) do not inhibit p53 interaction with DNA. **b**, Quantification of the pulldown experiment in **a**. The relative pulldown efficiency normalized to the input samples is shown on the *y* axis. The bar diagram shows the mean values and the error bars the corresponding s.d. of three biological replicates. An ordinary one-way ANOVA analysis was performed to assess the statistical significance (n.s., $P > 0.05$; $^{*}P \leq 0.05$, $^{**}P \leq 0.01$, $^{***}P \leq 0.001$, $^{****}P \leq 0.0001$). **c**, Crystal structure of DARPin C10 (blue) in complex with the p53 DBD (red) shown in two different orientations rotated by 90°. Top: cartoon representation. Bottom: space filling model. **d**, Comparison of a crystal structure of HPV E6 protein bound to the p53 DBD (PDB: 4XR8) (top) and the crystal structure of DARPin C10 bound to the p53 DBD (this work) (bottom). The DBD is shown in the same orientation. A comparison of both structures shows that DARPin C10 binds to the same region of the p53 DBD as HPV E6, thereby blocking the p53–E6 interaction. **e**, A superimposition of the crystal structure shown in **c** with a DNA complex indicates that DARPin C10 does not block the DNA-binding surface of the p53 DBD (PDB: 3KMD)[26]. **f**, A superimposition of the crystal structure shown in **c** with a crystal structure of the p53 DBD bound to a full consensus site as a self-assembled tetramer (PDB: 3KMD), suggesting that none of the DBD–DBD interfaces are blocked by DARPin binding.

its evolution—the E6 binding interface is accessible in both free and DNA-bound p53—could in principle be turned into its Achilles' heel by blocking this site for example with a DARPin. Here, we report the characterization of a DARPin that binds to the same site as the HPV E6 protein. In HPV-infected cells, this DARPin stabilized p53 and reactivated its transcriptional activity, including the initiation of apoptosis.

Results

DARPin C10 inhibits HPV E6 induced degradation of p53

To identify highly specific binders for the p53 DBD, we used a strategy similar to the one described previously for the selection of DARPins targeting the p63 domains[24] and the heterotetramer of p63 and p73 (ref. 25). Ribosome display[29] of the DARPin library was used for the selection of binders to the p53 DBD (amino acids 94–294), followed by screening of individual clones (Methods). Initial screening using homogeneous time-resolved fluorescence (HTRF) yielded several DARPins binding to the p53 DBD, which were counter-selected against binding to the DBDs of p63 and p73. Only monomeric DARPins without a tendency to aggregate were further considered. Three DARPins with quite different sequences, suggesting different binding sites on the p53 DBD, were further characterized for their ability to inhibit the degradation by the HPV16 E6 protein. To address this question, we used an in vitro degradation assay by expressing p53 in rabbit reticulocyte lysates (RRLs) followed by incubation with glutathione *S*-transferase (GST)-fused HPV16 E6 protein alone or GST-fused E6 protein and DARPin. As expected, incubation of p53 with HPV16 E6 led to the complete degradation of p53 within 180 min. The non-binding control DARPin E3_5 (ref. 30) had no inhibitory effect on this degradation (Fig. 1a,b). By contrast, DARPin C10

https://doi.org/10.1038/s41594-024-01456-7

efficiently inhibited degradation of p53, while other DARPins showed less or no protection (Extended Data Fig. 1a,b). Quantification of the protein level after 180 min indicated that incubation with DARPin C10 resulted in the same p53 level as in the GST-control sample, in which no degradation takes place (Fig. 1b). To investigate if the inhibitory effect is dependent on the HPV strain, we repeated the assay with HPV18-E6 and HPV35-E6, which returned the same results (Extended Data Fig. 1c,d). Based on these results, we decided to further concentrate on characterizing the DARPin C10.

We hypothesized that inhibition of degradation was most probably due to the displacement of the E6 protein from p53 by the DARPin. To verify this assumption, we performed a competitive pulldown assay in which biotinylated p53 DBD was immobilized on magnetic streptavidin beads and incubated with green fluorescent protein (GFP)-fused HPV16 E6 and the leucine-rich peptide of E6AP fused to the maltose binding protein that was used in structural studies before[13]. In addition, either no DARPin, the control DARPin or DARPin C10 were added. The pulldown of GFP-fused HPV16 E6 protein was detected for the samples containing no DARPin or the control DARPin, while coincubation with DARPin C10 resulted in a significant reduction of the interaction (Fig. 1c,d).

Affinity and selectivity of binding

We characterized the binding of DARPin C10 to the p53 DBD using isothermal titration calorimetry (ITC). Titration of the p53 DBD with DARPin C10 yielded a dissociation constant of K_d = 243 nM (Fig. 1e and Supplementary Table 1) at 25 °C or 180 nM at 15 °C (Extended Data Fig. 2a and Supplementary Table 1). Due to the high degree of sequence conservation in the DBDs of all p53 family members[31], we wanted to determine the specificity of this DARPin and measured binding to the DBDs of p63 and p73 as well but could not detect any interaction (Extended Data Fig. 2a). Titration of the DBDs of all p53 family members with a non-binding control DARPin did not show any interaction either (Extended Data Fig. 2b). Next, we investigated if the specific interaction of DARPin C10 with the p53 DBD is preserved in the context of the full-length protein in cell culture lysate. Hence, we overexpressed full-length p53, ΔNp63α and TAp73α in H1299 cells, and cell lysates were incubated with DARPin C10 or control DARPin immobilized on streptavidin magnetic beads. For DARPin C10, a strong pulldown of p53 was detected, while no interaction with ΔNp63α or TAp73α was observed. The control DARPin did not interact with any of the p53 family members (Fig. 1f).

Interaction interface of DARPin C10 on the p53 DBD

Protection from degradation is a necessary but not sufficient condition for reactivation of p53 in HPV-infected cells. Binding of the DARPin must also allow high-affinity binding of p53 to the DNA, which requires not only direct interaction with the DNA but also direct contacts between the DBDs that enable cooperative binding. We investigated if DARPin C10 interfered with these interactions by performing pulldown assays in which we incubated dsDNA comprising the human p21 promotor with p53 expressed in H1299 cells. Preincubation of the lysate with DARPin C10 or control DARPin did not result in a significant reduction of the pulldown efficiency compared with the pulldown without any DARPin (Fig. 2a,b). This result indicated that DARPin C10 recognizes an epitope on the DBD different from the epitope of the previously characterized DARPin G4 that blocks interaction with the DNA of all p53 family members[24].

To directly identify the interaction site of DARPin C10 on the p53 DBD, we determined a high-resolution (1.5 Å) crystal structure of the complex (Table 1, Fig. 2c and Extended Data Fig. 3a). This structure revealed that the interaction interface with DARPin C10 is located on the edge of the central β-sandwich, below the loop–sheet–helix motif, largely overlapping with the E6 binding site (Fig. 2d). A superimposition of the structure of the complex with a crystal structure of the p53 DBD bound to DNA (Protein Data Bank (PDB): 3KMD)[26]

Table 1 | Data collection and refinement statistics

	p53 DBD-C10	p53 DBD-C10-H82R
Data collection		
Space group	$P2_1$	$P2_1$
Cell dimensions		
a, b, c (Å)	37.69, 93.90, 53.17	37.71, 94.01, 53.17
α, β, γ (°)	90.00, 110.17, 90.00	90.00, 110.11, 90.00
Resolution (Å)	46.95–1.50 (1.53–1.50)[a]	47.01–1.44 (1.47–1.44)[a]
R_{merge}	0.062 (0.837)	0.045 (0.612)
$I/\sigma I$	13.8 (2.0)	12.5 (2.0)
Completeness (%)	98.6 (98.4)	98.8 (97.9)
Redundancy	5.7 (5.6)	3.8 (3.9)
Refinement		
Resolution (Å)	1.50	1.44
No. reflections	54,680	62,097
R_{work}/R_{free}	0.151/0.197	0.154/0.184
No. atoms		
Protein	2,484	2,487
Zinc ion	1	1
Ethylene glycol	16	12
Water	337	329
B factors		
Protein	24.7	25.8
Zinc ion	20.7	22.6
Ethylene glycol	48.4	44.3
Water	37.0	39.2
r.m.s.d.		
Bond lengths (Å)	0.005	0.005
Bond angles (°)	0.77	0.74

[a]Values in the parentheses are for highest-resolution shell. r.m.s.d., root mean square deviation.

(Fig. 2e,f) further indicated that the important DBD–DBD contacts, both within and between DNA half-sites, are not affected by binding of the DARPin. The p53–DARPin binding interface (with an interface area of 780 Å^2) is characterized by a central hydrophobic patch with three interacting tryptophan side chains, one from p53 and two from the DARPin (p53-Trp146, C10-Trp13 and C10-Trp46), flanked by intermolecular salt-bridge networks involving p53 residues Arg110 and Asp148 (Extended Data Fig. 3a). These key interacting residues are not conserved between p53 family members. Trp146 at the center of the interface, for example, is replaced by a lysine in p63 and p73, and the salt-bridge forming Arg110 is replaced by a negatively charged amino acid in the other two family members, explaining the high specificity of DARPin C10 for p53. Interestingly, the interacting tryptophan is conserved in the mouse p53 DBD, but there are three variations elsewhere in the interface region, with two of them affecting the above-mentioned intermolecular salt-bridge networks (Extended Data Fig. 3b). Consistent with this variation of two crucial residues in the interface region, no binding of DARPin C10 to the mouse DBD could be detected by ITC (Extended Data Fig. 3c).

DARPin C10 restores p53 activity in HPV-positive cell lines

Having shown that DARPin C10 protects p53 from degradation suggested that the transcriptional activity of p53 can be restored by the DARPin in HPV-infected cells. Therefore, we investigated the effect of DARPin C10 on the transcriptional activity of p53 in HeLa cells, which

https://doi.org/10.1038/s41594-024-01456-7

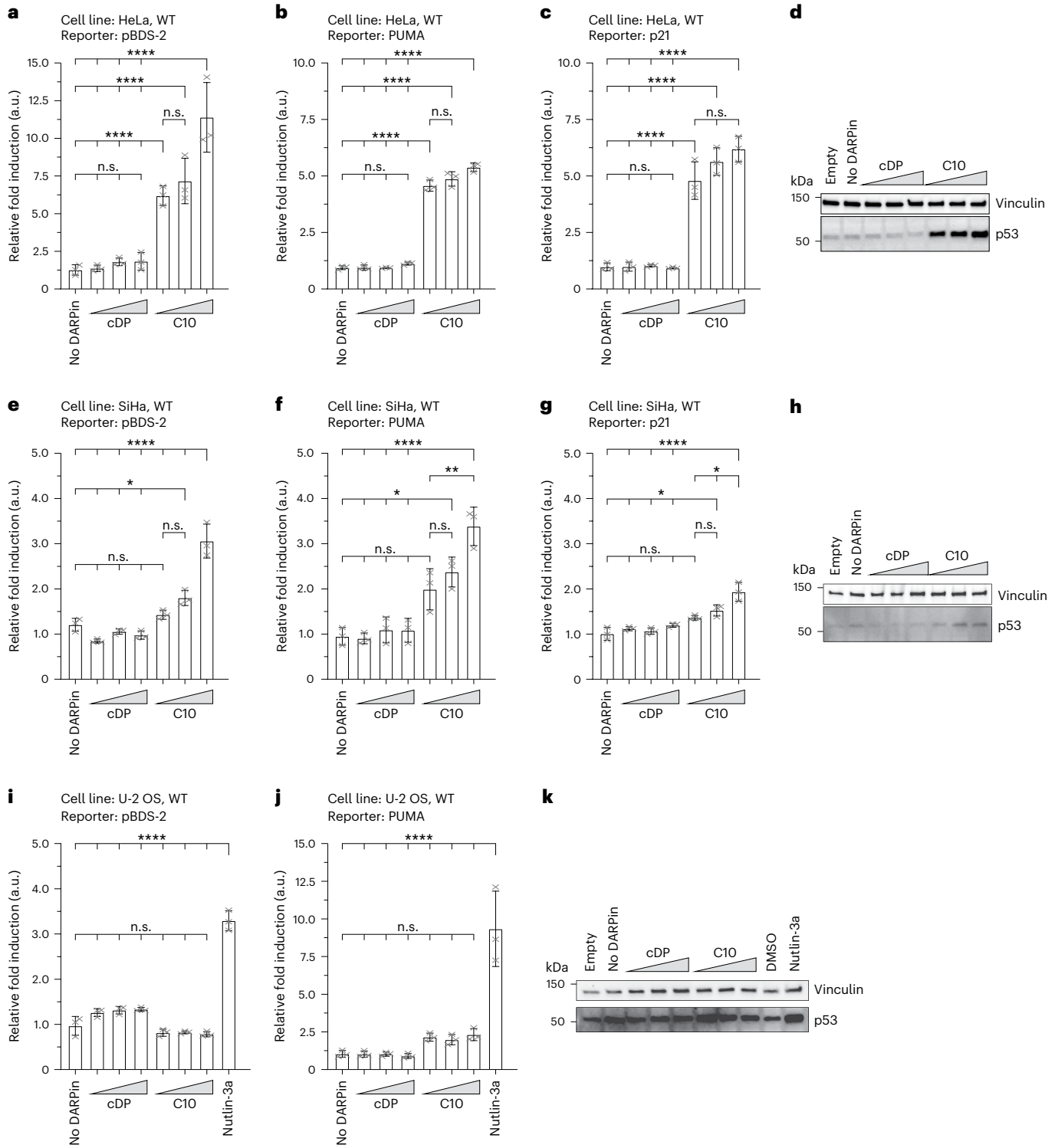

Fig. 3 | Reactivation of p53 by inhibition of its HPV-E6-mediated degradation. **a**, Transactivation assay in HPV18-positive HeLa cells with a luciferase expression construct under the control of a pBDS-2 promotor. Increasing amounts of DARPin C10 or control DARPin (cDP) were transiently transfected in HeLa cells. An increase in the transcriptional activity regulated by p53 can be observed with increasing amounts of DARPin C10, whereas the control DARPin had no effect. The bar diagram shows the mean values and the error bars the corresponding s.d. of three biological replicates. WT, wild type. **b**,**c**, The same assay as in **a** but with a luciferase expression construct under control of a PUMA promotor (**b**) or a p21 promotor (**c**). **d**, Exemplary western blot of the experiments in **a**–**c** detecting the p53 protein level using the α-p53 antibody DO-I (Santa Cruz Biotechnology). The level of vinculin served as a loading control. The expression of C10 led to a significant stabilization of p53. **e**–**h**, Same experiments as in **a**–**d** but with HPV16-positive SiHa cells instead of HPV18-positive HeLa cells. **i**,**j**, Transactivation assay with endogenous p53 in HPV-negative U-2 OS cells on the pBDS-2 promotor (**i**) and the PUMA promotor (**j**). The U-2 OS cells carry an amplification of the MDM2 gene, leading to degradation of p53. DARPin C10 does not interfere with the MDM2-mediated degradation of p53. The MDM2 inhibitor Nutlin-3a restores transcriptional activity of p53 by inhibiting its degradation. **k**, Exemplary western blot (out of three individual blots) of the experiments in **i** and **j** detecting the p53 protein level using the α-p53 antibody DO-I (Santa Cruz Biotechnology). The level of vinculin served as a loading control. DMSO, dimethyl sulfoxide. The experiments were performed in biological triplicates. The statistical significance was assessed by ordinary one-way ANOVA (n.s., $P > 0.05$; *$P \leq 0.05$, **$P \leq 0.01$, ***$P \leq 0.001$, ****$P \leq 0.0001$).

https://doi.org/10.1038/s41594-024-01456-7

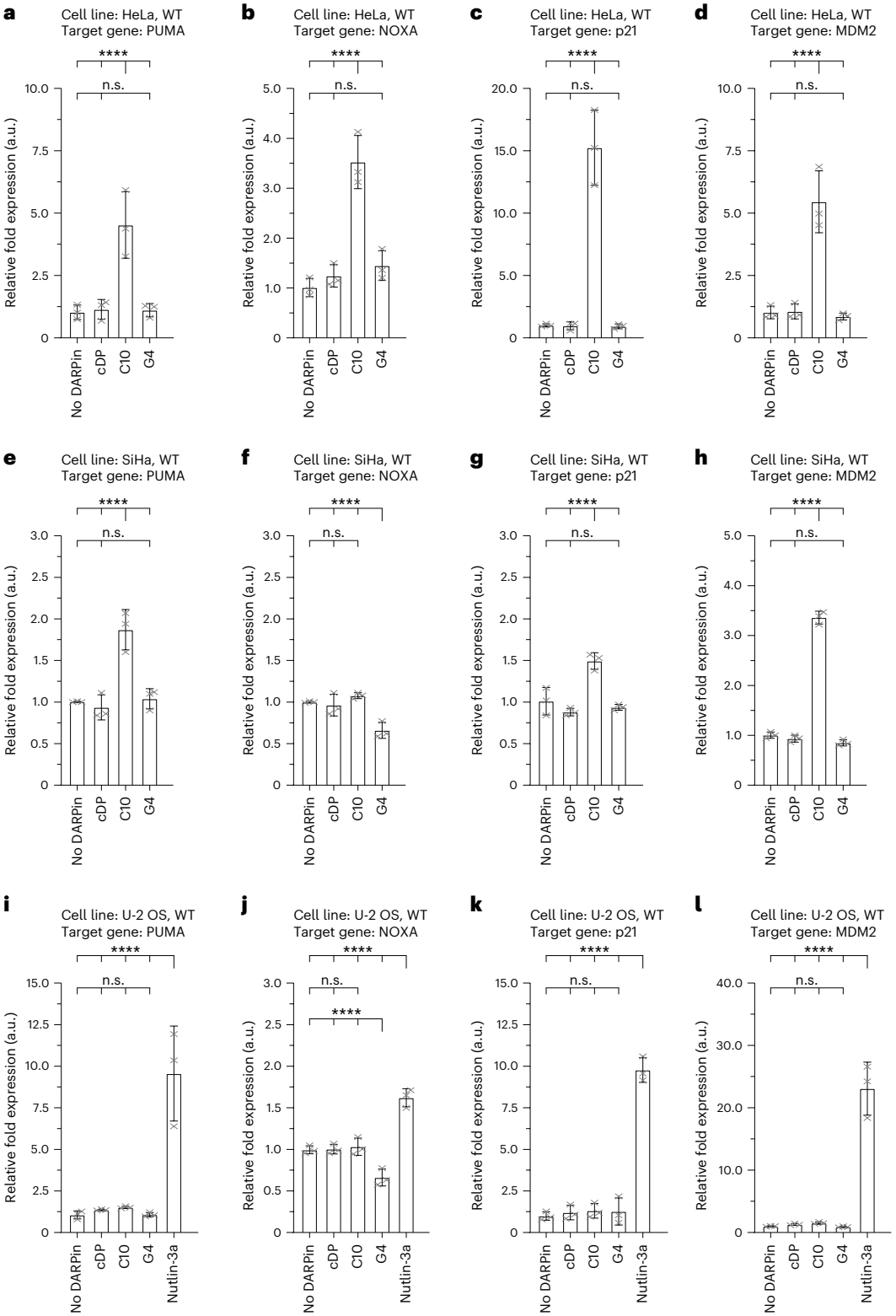

Fig. 4 | Reactivation of p53 in HPV-positive cells results in upregulation of proapoptotic p53 target genes. a, A reverse transcription qPCR (RT–qPCR) analysis of the expression of the PUMA gene in HPV18-positive HeLa cells expressing either no DARPin, control DARPin (cDP), DARPin C10 or the inhibitory DARPin G4. The total RNA was isolated from the cells and reverse transcribed into complementary DNA before analysis by qPCR. Gene expression was referenced to the housekeeping gene HPRT-1. WT, wild type. **b**–**d**, The same experiment as in **a** but with the p53 target genes NOXA (**b**), p21 (**c**) and MDM2 (**d**). **e**–**h**, An RT–qPCR analysis of the expression of the p53 target genes PUMA (**e**), NOXA (**f**), p21 (**g**) and MDM2 (**h**) in HPV16-positive SiHa cells expressing either no DARPin, control DARPin, DARPin C10 or the inhibitory DARPin G4. **i**–**l**, The same experiment as in **a**–**d** but with HPV-negative U-2 OS cells carrying an amplification of the MDM2 gene, leading to degradation of p53. DARPin C10 does not interfere with the MDM2-mediated degradation of p53. In **a**–**l**, the bar diagrams show the mean values and the error bars the corresponding s.d. of three biological replicates. An ordinary one-way ANOVA was performed to assess the statistical significance (n.s., $P > 0.05$; *$P \leq 0.05$, **$P \leq 0.01$, ***$P \leq 0.001$, ****$P \leq 0.0001$).

https://doi.org/10.1038/s41594-024-01456-7

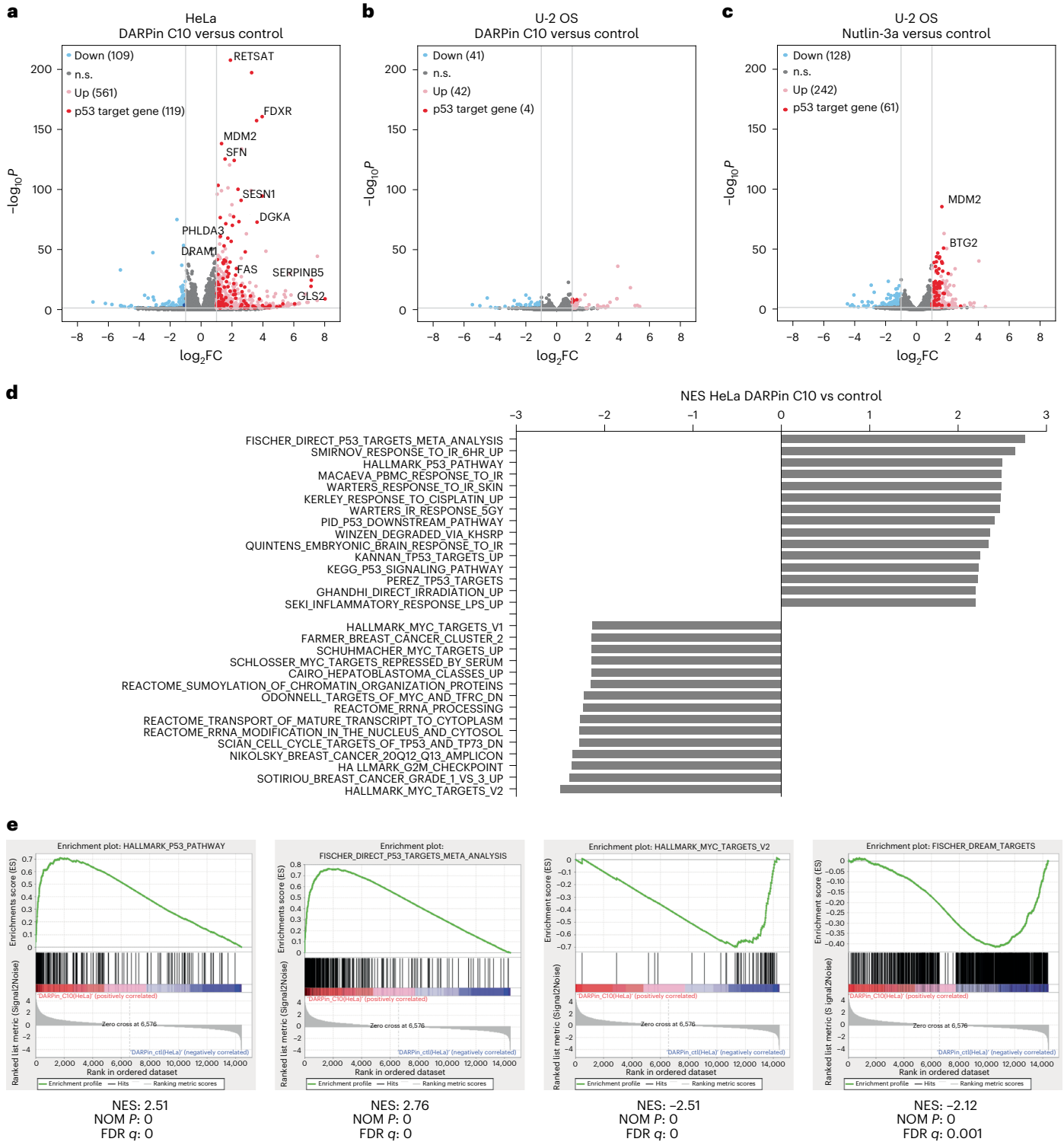

Fig. 5 | RNA-seq. a–**c**, Volcano plots showing differentially regulated genes in the indicated pair-wise comparisons in DARPin-expressing HeLa cells (**a**), DARPin-expressing U-2 OS cells (**b**) and Nutlin-3a treated U-2 OS cells (**c**) using a fold change of 2 (abs(log_2FC) >1) and an adjusted *P* value <0.05 as significance thresholds. Significantly downregulated genes are colored in light blue and upregulated genes in light red, and their numbers are stated in parentheses. Significantly upregulated genes included in the HALLMARK_P53_PATHWAY or FISCHER_DIRECT_P53_TARGETS_META_ANALYSIS gene sets (MSigDB, version 7.1) are shown in red. The gene name labels identify selected p53 target genes. The significance was assessed by using a two-sided Wald test with adjusting via a Benjamini–Hochberg procedure. **d**,**e**, GSEA results of HeLa cells expressing DARPin C10 versus control; the bar graph shows the normalized enrichment scores (NES) for the top 15 enriched or depleted gene sets from the H, C2, C6 and C7 MSigDB collections (**d**), and the enrichment plots show exemplary p53-related MSigDB gene sets with their NES, nominal *P* value (NOM *P*) and FDR *q* value (FDR *q*) (**e**).

are HPV18-positive[32]. For this purpose, a luciferase-based transactivation assay was performed by transient cotransfection of empty pcDNA3.1(+) plasmid or plasmids coding for DARPin C10 or the control DARPin together with the respective reporter plasmids into HeLa cells. No transactivation on the pBDS-2, PUMA or p21 promotor was observed for the samples containing empty vector or control DARPin, while increasing transcriptional activity was observed with increasing amounts of DARPin C10 on all promotors (Fig. 3a–c). Additionally, the

p53 protein level was monitored by western blot. Nearly no p53 could be detected in samples containing no DARPin or control DARPin. However, a significant stabilization of p53 was observed already with the lowest transfected amount of DARPin C10 (100 ng plasmid DNA), which further increased with increasing amounts of DARPin C10 (Fig. 3d). The assay was repeated using SiHa cells, which are HPV16-positive[33]. Similarly to the HeLa cells, increasing transactivation was observed with increasing amounts of DARPin C10, but the overall activity was lower compared with HeLa cells (Fig. 3e–g). This also correlated with a lower p53 protein level observed by western blot (Fig. 3h). The transactivation assay was repeated with HPV-negative U-2 OS cells to eliminate the possibility that DARPin C10 interfered with the MDM2 feedback loop. In this assay, treatment of the cells with the MDM2 inhibitor Nutlin-3a for 6 h was included as a positive control. Transient expression of DARPin C10 in those cells did not lead to significantly higher transactivation compared with samples containing no DARPin or control DARPin, while treatment with Nutlin-3a resulted in drastically increased transactivation (Fig. 3i,j). Furthermore, no stabilization of p53 on the protein level was observed for control DARPin or DARPin C10, while a significantly higher protein level was observed after treatment with Nutlin-3a (Fig. 3k). These results indicate that DARPin C10 is a potent reactivator of p53 in HPV-positive cells, without interfering with the MDM2 feedback loop.

To further characterize the reactivation of p53 regarding other proapoptotic target genes, we performed real-time quantitative polymerase chain reaction (PCR). Control DARPin, DARPin C10 or DARPin G4, which inhibits p53's transcriptional activity[24], were transiently transfected in HeLa (HPV18-positive), SiHA (HPV16-positive) or U-2 OS (HPV-negative) cells, and the total messenger RNA was extracted 24 h after transfection. The cells transfected with empty pcDNA3.1(+) vector served as a reference. In the case of the HeLa cells, expression of DARPin C10 led to a significant increase of the expression of the p53 target genes PUMA, NOXA, p21 and MDM2, while the non-binding control DARPin and the inhibitory DARPin G4 had no effect (Fig. 4a–d). In SiHa cells, a significant increase of p53 target gene expression was observable for PUMA, p21 and MDM2 but not for NOXA (Fig. 4e–h). However, the fold change was much lower than in the experiments performed with the HeLa cells. The control DARPin had no effect, while expression of the inhibitory DARPin G4 led to a slightly reduced expression of NOXA (Fig. 4f). The experiment was repeated with HPV-negative U-2 OS cells as well. No change of the fold expression of the p53 target genes was observed for the control DARPin and DARPin C10, while expression of DARPin G4 led to a reduced expression of NOXA (Fig. 4i–l). Overall, these experiments convincingly showed that DARPin C10 is a potent reactivator of p53 activity in HPV-positive cells that does not interfere with the important regulatory MDM2 negative feedback loop.

DARPin C10 reactivated p53-dependent transcription

p53 regulates several hundred target genes beyond p21, MDM2, PUMA and NOXA that synergistically contribute to its tumor-suppressive activity[34,35]. We, therefore, profiled the transcriptional changes induced by DARPin C10 in HPV-positive HeLa and HPV-negative U-2 OS cells by RNA sequencing (RNA-seq) using the non-binding DARPin as a negative and Nutlin-3a as a positive control. DARPin C10 induced profound transcriptional alterations in HeLa cells, with a total of 561 genes significantly upregulated and 109 genes downregulated (Fig. 5a). In HPV-negative U-2 OS cells, a similar reprogramming of the transcriptome was only observed in response to Nutlin-3a treatment but not by expression of DARPin C10 (Fig. 5b,c). Many of the genes activated by DARPin C10 in HeLa cells are canonical p53 target genes, including MDM2, BTG2, FAS and FDXR (Fig. 5a and Supplementary Table 2). Moreover, Gene Set Enrichment Analysis (GSEA) identified various p53 target gene sets and p53-related DNA damage signatures as the most significantly upregulated pathways (Fig. 5d,e). Consistent with p53-mediated repression of cell-cycle genes via the DREAM complex[36,37], various Myc-regulated cell-cycle gene sets were among the most strongly depleted signatures.

Expression of DARPin C10 resulted in reduced cell viability

The question arose whether expression of DARPin C10 also results in reduced cell viability. Immunofluorescence (IF) was measured to assess expression and nuclear localization of the DARPins. IF staining of HeLa cells showed that the DARPins were mainly located in the nucleus (Fig. 6a,b). Furthermore, p53 expression was detected in cells that expressed DARPin C10. The same experiment was performed with SiHa cells, leading to the same result (Fig. 6c,d). However, the p53 protein level in the nucleus was lower compared with that in HeLa cells. As a control, HPV-negative U-2 OS cells expressing DARPin C10 or control DARPin were generated. IF staining indicated that both DARPins were present in the nucleus of these cells as well, but no increase of p53 protein level was detected (Fig. 6e,f). The cell viability was measured for 80 h, revealing that HeLa cells expressing DARPin C10 proliferated at similar level compared with cells expressing control DARPin in the first few hours, but then, cell growth slowed down, and cell viability began to decrease. By contrast, no reduction of cell viability was detectable for cells expressing control DARPin over the entire experimental period (Fig. 6g). In comparison with HeLa cells, SiHa cells grew more slowly. For cells expressing DARPin C10, a reduction of cell viability was detectable after approximately 50 h, while the cells expressing control DARPin continued to grow (Fig. 6h). HPV-negative U-2 OS cells served as a negative control, showing a slight reduction of the proliferation rate but no reduction of cell viability for cells expressing either control DARPin or DARPin C10, suggesting that none of the DARPins caused toxicity in these cells (Fig. 6i).

Delivery of DARPins via a messenger RNA/lipid nanoparticle approach

The use of biotherapeutics such as DARPins in the clinic has so far been limited to extracellular applications (see 'Discussion'), as their intracellular application is hampered by their inability to cross biological membranes, requiring delivery systems for the DARPin or its genetic information. A variety of viral and non-viral gene delivery systems have been developed[38,39], both for DNA and for RNA. One of the non-viral methods is the delivery of mRNA packaged in lipid nanoparticles that has been used for vaccine delivery. Its use for the delivery of

Fig. 6 | Reactivation of p53 in HPV-positive cells results in a decreased cell viability. a, IF staining to analyze expression of p53 in HeLa cells stably expressing DARPin C10 (left) or control DARPin (cDP) (right). The cells were fixed with formaldehyde and incubated with anti-Myc (Abcam) antibody to detect DARPin expression and α-p53 antibody DO-I (Santa Cruz Biotechnology) to detect p53 expression, followed by incubation with the secondary antibodies Alexa Fluor 568 anti-rabbit (Life Technologies) and Alexa Fluor 647 anti-mouse (Life Technologies). DNA was stained with 4′,6-diamidino-2-phenylindole (DAPI). Scale bar, 20 µm. **b**, A quantification of the p53 protein level detected in **a**. The bar diagrams represent the mean value of four individual images used for the analysis and error bars depict the corresponding s.d. An ordinary one-way ANOVA was performed to assess the statistical significance (n.s., $P > 0.05$; *$P \leq 0.05$, **$P \leq 0.01$, ***$P \leq 0.001$, ****$P \leq 0.0001$). **c**–**f**, Same experiment as in **a** but with SiHa cells stably expressing C10 (**c**) or control DARPin (**d**) or U-2 OS cells stably expressing either C10 (**e**) or control DARPin (**f**). **g**, Cell viability of HeLa cells stably expressing DARPin C10 (red) or control DARPin (blue). The viability was monitored over 80 h using the Real Time Glo MT cell viability assay (Promega). The cells expressing DARPin C10 showed a significantly reduced cell viability. **h**, Same assay as in **g** but with HPV16-positive SiHa cells. Again, the cells expressing C10 showed a significantly decreased viability compared with cells expressing control DARPin. **i**, Same assay as in **g** but with HPV-negative U-2 OS cells that carry an amplification of the MDM2 gene, leading to degradation of p53. DARPin C10 had no significant impact on the viability of these cells. All data were normalized to the cell viability after 1 h. The standard deviations of biological triplicates are shown by dotted lines.

https://doi.org/10.1038/s41594-024-01456-7

therapeutics, requiring much higher concentrations than vaccines, is still in early stages of development[40]. As a proof of principle that such an approach can work, we have generated mRNA from the expression plasmid of the DARPin C10 as well as from the control DARPin and a GFP expression plasmid. For higher stability, the mRNA contained pseudouridine and 5-methyl cytosine[41]. Transient transfection of HeLa, SiHa and U-2 OS cells with mRNA packaged in Lipofectamine MessengerMax (Invitrogen) showed a very high transfection efficiency. IF staining revealed stabilization of p53 in HeLa and SiHa cells transfected with DARPin C10 but not with the control DARPin. In U-2 OS cells, the stabilizing effect was minimal (Extended Data Fig. 4a–f). A quantitative PCR (qPCR) analysis of selected p53 target genes in the transfected HeLa cells demonstrated an upregulation of the genes coding for PUMA, NOXA, p21 and Mdm2 (Extended Data Fig. 4g–j).

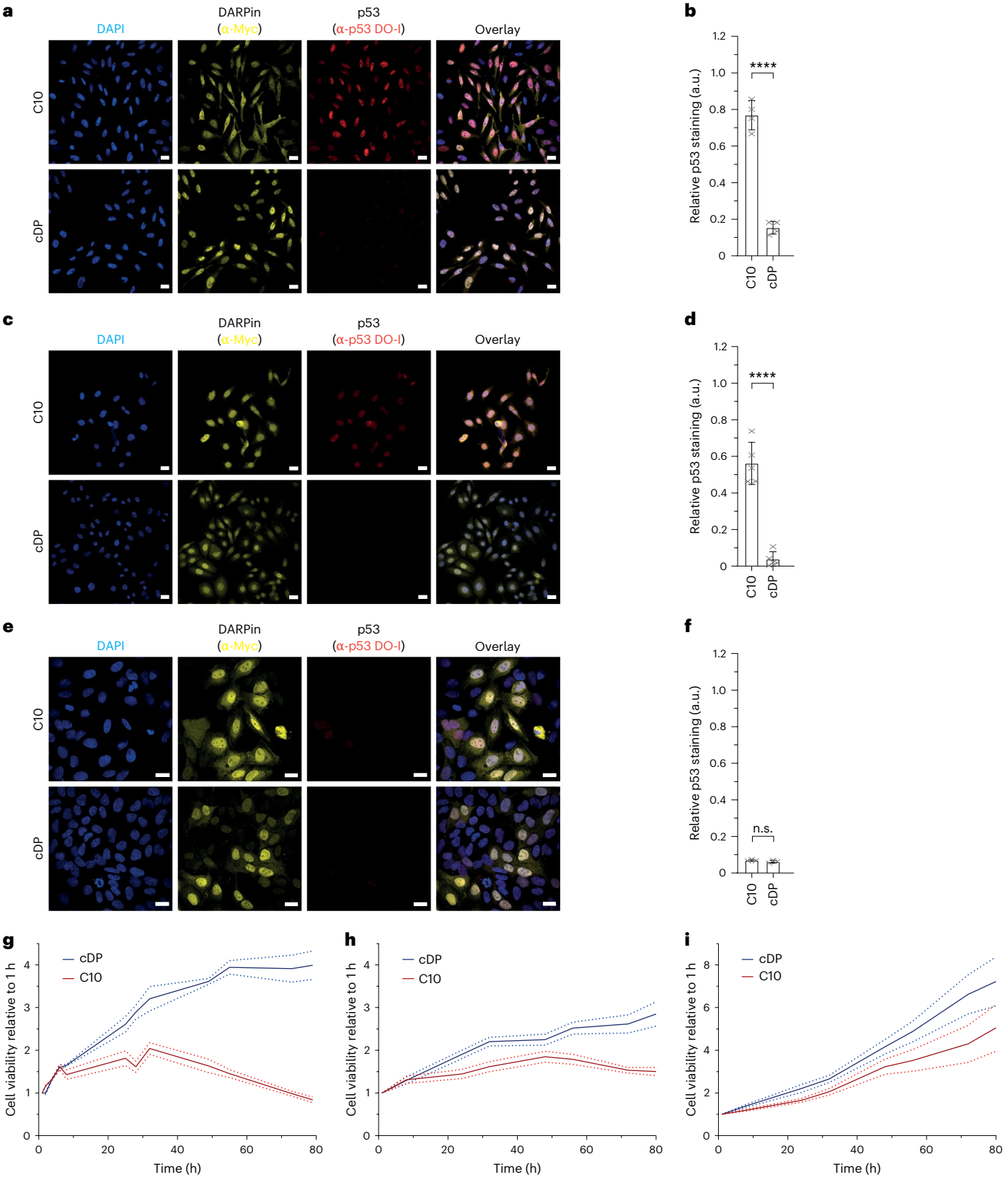

https://doi.org/10.1038/s41594-024-01456-7

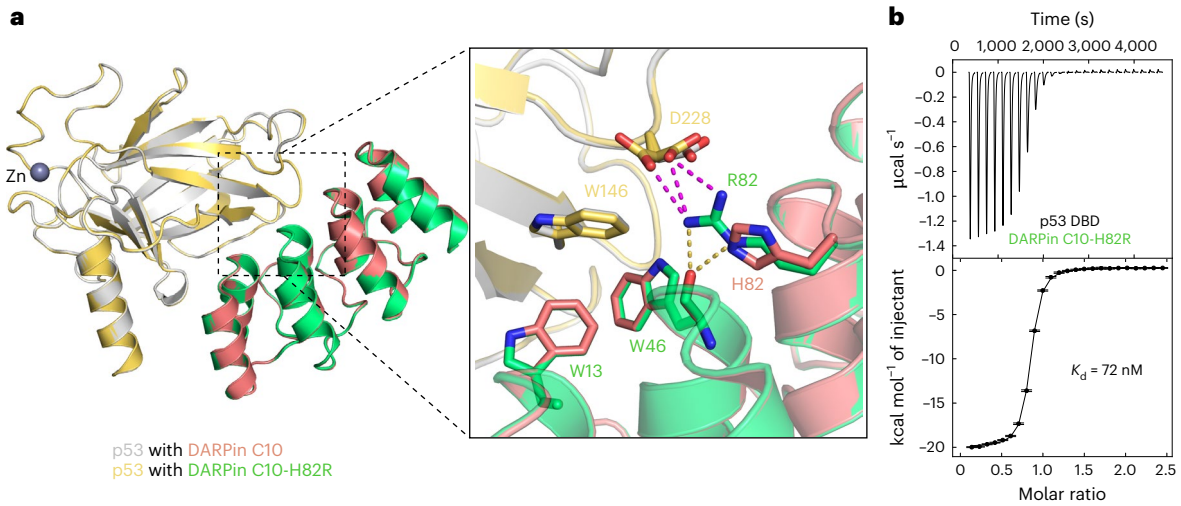

Fig. 7 | Structure-guided optimization of DARPin C10. a, A superimposition of the p53 DBD complex with DARPin C10 and the C10-H82R mutant showing the engineered intermolecular salt bridge on the edge of the p53-DARPin interface between Arg82 and p53 residue Asp228 (highlighted with magenta broken lines). Intramolecular hydrogen bonds mediated by the Arg82 side chain are shown as orange broken lines. Asp228 adopts two alternative conformations in the complex with the mutant DARPin. **b**, ITC data for binding of the human p53 DBD to the second-generation variant C10-H82R DARPin, showing a 3.5-fold increase in binding affinity relative to the affinity of the original DARPin C10 (Fig. 1e). All ITC measurements were performed at 25 °C as technical duplicates with one being shown. The error bars represent the error of the fitting procedure.

Structure-based design of the interface improves affinity

With a K_d of 250 nM, the affinity of DARPin C10 to the p53 DBD is relatively weak. A detailed analysis of the C10–p53 interface suggested a mutation for extending the interface and potentially improving affinity, by engineering an additional intermolecular salt bridge by mutating His82 to an arginine. Gratifyingly, the C10-H82R mutant bound the p53 DBD with a K_d of 72 nM, which corresponds to a 3.5-fold affinity increase, and the 1.4 Å crystal structure of the mutant complex confirmed the formation of the anticipated salt bridge between Arg82 and p53 residue Asp228 (Fig. 7a,b).

We wanted to test if the enhanced affinity of DARPin C10-H82R would also directly translate into a higher transcriptional activity of p53. Transfecting HeLa cells transiently with DARPin C10-H82R mRNA resulted indeed in a higher p53 level and significantly higher transcript levels of all tested p53 target genes (Extended Data Fig. 5). We also compared the effect of expressing the DARPin in HeLa cells with that using short interfering RNA (siRNA) targeting the HPV18 E6 protein. As expected, the knockdown of the E6 protein resulted in stabilization of p53 and in an increase in p53 target gene expression. However, for all investigated p53 target genes this effect was significantly lower than their DARPin-induced upregulation (Extended Data Fig. 5). Taken together, these data showed that DARPin-induced reactivation of p53 in HPV18-positve HeLa cells is more efficient than siRNA-mediated knockdown of HPV E6. In SiHa cells, we also confirmed the higher activation level of DARPin C10-H82R compared with C10. As noted before, the overall effect of the DARPins were smaller than in the HeLa cells. Surprisingly, using siRNA targeting the HPV16 E6 protein had almost no effect on stabilizing p53 (Extended Data Fig. 6).

To investigate if expression of the DARPin induces apoptosis or only cell-cycle arrest, we probed the integrity of the cellular membrane and the activity of caspases 3 and 7. In HeLa cells, a strong increase in the apoptotic signals after 48 h expression of DARPin C10 was seen that was even higher for the optimized DARPin C10-H82R. Similar but smaller effects were measured in SiHa cells (Extended Data Fig. 7).

Discussion

Inhibition of protein–protein interactions by small molecules is notoriously difficult, as these interactions are typically mediated by relatively large surfaces that lack distinct binding pockets for small molecules. By contrast, designed macromolecules can provide the required large surfaces and can be developed into highly affine and selective inhibitors with well-established in vitro evolution and selection methods such as ribosome or phage display. Proteins in general have the advantage over RNA aptamers in that they can bind to a much higher diversity of epitopes, as they do not need to contain an extremely high number of negative charges.

The high potential of protein therapeutics can be seen from the enormous success of antibodies targeting cell-surface receptors, for example in cancer therapy. Nonetheless, most proteins do not cross the cell membrane. Many attempts in the past were based on engineering features into proteins that would enhance cell permeability[42]. A prominent example are cell-penetrating peptide tags[43,44], but their efficacy is very limited, and their typically high positive charge leads to unspecific binding to serum proteins[45]. Both viral vectors and non-viral vectors are under development, and both DNA and RNA is being considered as the genetic material. Viral vectors can be targeted to specific surface receptors[46,47] and, thus, to specific cell types.

Since the severe acute respiratory syndrome coronavirus 2 pandemic, another promising approach to deliver proteins into the cellular cytoplasm has emerged: mRNA packaged into lipid nanoparticles. While this technology has so far mainly been used to develop vaccines, it also holds the potential to deliver mRNA for proteins into cells. However, there are several important challenges for a therapeutic that are different from a vaccine[40]: (1) the amount of protein needed for therapy is several orders of magnitude greater than for a vaccine, (2) the required duration for the action of the payload protein is typically much longer for a therapeutic than for a vaccine and (3) usually, the payload expression should be limited to specific cell types as it may be harmful when expressed in healthy tissue. The success of such an approach will, thus, certainly depend on the tissue type to be targeted. Lipid nanoparticles are, for example, known to accumulate in the liver, making this organ a potentially better target than others[48]. This has recently been demonstrated by the first results of a phase 1/2 clinical trial for the treatment of propionic acidaemia, a metabolic disease in which defects in the propionyl-coenzyme A carboxylase result in the buildup of toxic metabolites. Treatment of patients with mRNA/lipid nanoparticles resulted in up to 70% reduction in the risk of metabolic decompensation events[49]. This clinical trial has also shown that

relatively high doses of LNPs over long periods of time are safe for humans. Recent development of lipids for LNP treatment has shown that other organs such as the lung or spleen can be targeted as well, making selective targeting possible[50,51]. Yet other potential applications could be in organs that can easily be reached and treated locally with higher concentrations. HPV induces tumors in keratinized and mucosal epithelia, which are in principle surface exposed. This opens the possibility to treat affected regions with lipid nanoparticles containing the mRNA of a DARPin that prevents degradation of p53. In this study, we have characterized a potential candidate and shown that the DARPin C10 effectively reactivates p53 in HPV-infected cells by displacing the viral E6 protein from the p53 DBD.

The DARPin described here does not inhibit the disease-causing protein, in this case, the viral E6 protein, but indirectly prevents its action. This approach has a potential risk but also certain advantages. The risk is that p53 is stabilized also in healthy cells, especially when using a non-targeted gene delivery approach, resulting in unwanted activation and possibly toxicity. Our investigations in U-2 OS cells that have wild-type p53 and are not HPV-infected have so far shown that the DARPin does not interfere with the important MDM2 negative feedback loop. However, further investigations including RNA-seq experiments in primary tissues will be necessary to evaluate the safety of this DARPin in more detail. The advantage of the DARPin binding to the p53 DBD is that it displaces the E6 proteins of all HPV subtypes. This is of interest because the currently used vaccination is only effective for some HPV strains[52]. Our results have, however, also shown that reactivation of p53 in HPV18-infected cells seems easier than in HPV16-infected ones. This correlates with and might be due to the higher affinity of the HPV16 E6 protein to p53 compared with the HPV18 E6 protein[4,53]. Further improvement of the affinity of the DARPin to p53 will further improve its protective effect.

The alternative strategy of blocking the function of the E6 protein with an inhibitor that directly binds to the E6 protein could result in less effective protection against some subtypes, despite the high sequence conservation of the E6 proteins. The second advantage of the currently chosen strategy over developing an inhibitor of E6 is that binding of such an inhibitor to E6 would probably also stabilize the E6 protein. This might lead to higher cellular concentrations with unpredictable side effects, as the E6 protein not only binds to the p53 DBD but also has many other cellular interaction partners[7]. It has, for example, been shown that binding of a leucine-rich peptide mimicking the interaction peptide of the E6AP protein not only prevents degradation of p53 but also stabilizes HPV16 E6 (ref. 54).

One general potential disadvantage of protein pharmaceuticals is that they can lead to an unwanted immune reaction. DARPins have already entered clinical trials. The scaffold of DARPins is not prone to aggregate[21], and low aggregation propensity has been shown to inversely correlate with the immunogenic potential of a therapeutic protein[55]. The immunogenic potential of DARPins was tested in a first-in-human study of MP0250, a DARPin drug candidate inhibiting vascular endothelial growth factor and hepatocyte growth factor, where the absence of clearing antibodies was found, despite some levels of antidrug antibodies in some patients[56]. The data available so far predict that DARPins have a low risk of inducing a severe immune response, but this will have to be established for the actual DARPin of interest. As many human ankyrin repeat proteins exist, it is also possible to partially 'humanize' DARPins, similarly to the successful humanization of antibodies that has already proven successful in many applications in patients.

Online content

Any methods, additional references, Nature Portfolio reporting summaries, source data, extended data, supplementary information, acknowledgements, peer review information; details of author contributions and competing interests; and statements of data and code availability are available at https://doi.org/10.1038/s41594-024-01456-7.

References

1. zur Hausen, H. Immortalization of human cells and their malignant conversion by high risk human papillomavirus genotypes. *Semin. Cancer Biol.* **9**, 405–411 (1999).
2. de Martel, C., Plummer, M., Vignat, J. & Franceschi, S. Worldwide burden of cancer attributable to HPV by site, country and HPV type. *Int J. Cancer* **141**, 664–670 (2017).
3. Hufbauer, M. & Akgul, B. Molecular mechanisms of human papillomavirus induced skin carcinogenesis. *Viruses* **9**, 187 (2017).
4. Scheffner, M., Werness, B. A., Huibregtse, J. M., Levine, A. J. & Howley, P. M. The E6 oncoprotein encoded by human papillomavirus types 16 and 18 promotes the degradation of p53. *Cell* **63**, 1129–1136 (1990).
5. Huibregtse, J. M., Scheffner, M. & Howley, P. M. A cellular protein mediates association of p53 with the E6 oncoprotein of human papillomavirus types 16 or 18. *EMBO J.* **10**, 4129–4135 (1991).
6. McLaughlin-Drubin, M. E. & Münger, K. The human papillomavirus E7 oncoprotein. *Virology* **384**, 335–344 (2009).
7. Tungteakkhun, S. S. & Duerksen-Hughes, P. J. Cellular binding partners of the human papillomavirus E6 protein. *Arch. Virol.* **153**, 397–408 (2008).
8. Helt, A. M. & Galloway, D. A. Mechanisms by which DNA tumor virus oncoproteins target the Rb family of pocket proteins. *Carcinogenesis* **24**, 159–169 (2003).
9. Dyson, N., Guida, P., Munger, K. & Harlow, E. Homologous sequences in adenovirus E1a and human papillomavirus E7 proteins mediate interaction with the same set of cellular proteins. *J. Virol.* **66**, 6893–6902 (1992).
10. Liu, Y. Q., Cherry, J. J., Dineen, J. V., Androphy, E. J. & Baleja, J. D. Determinants of stability for the E6 protein of papillomavirus type 16. *J. Mol. Biol.* **386**, 1123–1137 (2009).
11. Zanier, K. et al. Solution structure analysis of the HPV16 E6 oncoprotein reveals a self-association mechanism required for E6-mediated degradation of p53. *Structure* **20**, 604–617 (2012).
12. Zanier, K. et al. Structural basis for hijacking of cellular LxxLL motifs by papillomavirus E6 oncoproteins. *Science* **339**, 694–698 (2013).
13. Martinez-Zapien, D. et al. Structure of the E6/E6AP/p53 complex required for HPV-mediated degradation of p53. *Nature* **529**, 541–545 (2016).
14. Münger, K. et al. Mechanisms of human papillomavirus-induced oncogenesis. *J. Virol.* **78**, 11451–11460 (2004).
15. Hudson, J. B., Bedell, M. A., McCance, D. J. & Laiminis, L. A. Immortalization and altered differentiation of human keratinocytes in vitro by the E6 and E7 open reading frames of human papillomavirus type 18. *J. Virol.* **64**, 519–526 (1990).
16. Hawleynelson, P., Vousden, K. H., Hubbert, N. L., Lowy, D. R. & Schiller, J. T. Hpv16 E6-proteins and E7-proteins cooperate to immortalize human foreskin keratinocytes. *EMBO J.* **8**, 3905–3910 (1989).
17. Celegato, M. et al. A novel small-molecule inhibitor of the human papillomavirus E6-p53 interaction that reactivates p53 function and blocks cancer cells growth. *Cancer Lett.* **470**, 115–125 (2020).
18. Wang, J. C. K. et al. Structure of the p53 degradation complex from HPV16. *Nat. Commun.* **15**, 1842 (2024).
19. Ramirez, J. et al. Targeting the two oncogenic functional sites of the HPV E6 oncoprotein with a high-affinity bivalent ligand. *Angew. Chem. Int. Ed. Engl.* **54**, 7958–7962 (2015).
20. Boersma, Y. L. & Pluckthun, A. DARPins and other repeat protein scaffolds: advances in engineering and applications. *Curr. Opin. Biotechnol.* **22**, 849–857 (2011).
21. Pluckthun, A. Designed ankyrin repeat proteins (DARPins): binding proteins for research, diagnostics, and therapy. *Annu. Rev. Pharmacol. Toxicol.* **55**, 489–511 (2015).

22. Binz, H. K. et al. High-affinity binders selected from designed ankyrin repeat protein libraries. *Nat. Biotechnol.* **22**, 575–582 (2004).
23. Dreier, B., Plückthun, A. in *Ribosome Display and Related Technologies. Methods in Molecular Biology* Vol. 805 (eds Douthwaite, J. & Jackson, R.) 261–286 (Springer, 2012).
24. Strubel, A. et al. Designed Ankyrin Repeat Proteins as a tool box for analyzing p63. *Cell Death Differ.* **29**, 2445–2458 (2022).
25. Strubel, A. et al. DARPins detect the formation of hetero-tetramers of p63 and p73 in epithelial tissues and in squamous cell carcinoma. *Cell Death Dis.* **14**, 674 (2023).
26. Chen, Y. H., Dey, R. & Chen, L. Crystal structure of the p53 core domain bound to a full consensus site as a self-assembled tetramer. *Structure* **18**, 246–256 (2010).
27. Dehner, A. et al. Cooperative binding of p53 to DNA: regulation by protein-protein interactions through a double salt bridge. *Angew. Chem. Int. Ed. Engl.* **44**, 5247–5251 (2005).
28. Kitayner, M. et al. Diversity in DNA recognition by p53 revealed by crystal structures with Hoogsteen base pairs. *Nat. Struct. Mol. Biol.* **17**, 423–429 (2010).
29. Plückthun, A. in *Ribosome Display and Related Technologies. Methods in Molecular Biology* Vol. 805 (eds Douthwaite, J. & Jackson, R.) 3–28 (Springer, 2012).
30. Binz, H. K., Stumpp, M. T., Forrer, P., Amstutz, P. & Plückthun, A. Designing repeat proteins: well-expressed, soluble and stable proteins from combinatorial libraries of consensus ankyrin repeat proteins. *J. Mol. Biol.* **332**, 489–503 (2003).
31. Osterburg, C. & Dotsch, V. Structural diversity of p63 and p73 isoforms. *Cell Death Differ.* **29**, 921–937 (2022).
32. Schwarz, E. et al. Structure and transcription of human papillomavirus sequences in cervical-carcinoma cells. *Nature* **314**, 111–114 (1985).
33. Yee, C., Krishnanhewlett, I., Baker, C. C., Schlegel, R. & Howley, P. M. Presence and expression of human papillomavirus sequences in human cervical-carcinoma cell lines. *Am. J. Pathol.* **119**, 361–366 (1985).
34. Fischer, M. Census and evaluation of p53 target genes. *Oncogene* **36**, 3943–3956 (2017).
35. Kastenhuber, E. R. & Lowe, S. W. Putting p53 in context. *Cell* **170**, 1062–1078 (2017).
36. Fischer, M., Grossmann, P., Padi, M. & DeCaprio, J. A. Integration of TP53, DREAM, MMB-FOXM1 and RB-E2F target gene analyses identifies cell cycle gene regulatory networks. *Nucleic Acids Res.* **44**, 6070–6086 (2016).
37. Schade, A. E., Fischer, M. & DeCaprio, J. A. RB, p130 and p107 differentially repress G1/S and G2/M genes after p53 activation. *Nucleic Acids Res.* **47**, 11197–11208 (2019).
38. Dogbey, D. M. et al. Technological advances in the use of viral and non-viral vectors for delivering genetic and non-genetic cargos for cancer therapy. *Drug Deliv. Transl. Res.* **13**, 2719–2738 (2023).
39. Singh, V., Khan, N. & Jayandharan, G. R. Vector engineering, strategies and targets in cancer gene therapy. *Cancer Gene Ther.* **29**, 402–417 (2022).
40. Rohner, E., Yang, R., Foo, K. S., Goedel, A. & Chien, K. R. Unlocking the promise of mRNA therapeutics. *Nat. Biotechnol.* **40**, 1586–1600 (2022).
41. Sahin, U., Karikó, K. & Türeci, Ö. mRNA-based therapeutics—developing a new class of drugs. *Nat. Rev. Drug Discov.* **13**, 759–780 (2014).
42. Deprey, K., Becker, L., Kritzer, J. & Plückthun, A. Trapped! A critical evaluation of methods for measuring total cellular uptake versus cytosolic localization. *Bioconjugate Chem.* **30**, 1006–1027 (2019).
43. Ramaker, K., Henkel, M., Krause, T., Röckendorf, N. & Frey, A. Cell penetrating peptides: a comparative transport analysis for 474 sequence motifs. *Drug Deliv.* **25**, 928–937 (2018).
44. Peraro, L. & Kritzer, J. A. Emerging methods and design principles for cell-penetrant peptides. *Angew. Chem. Int. Ed.* **57**, 11868–11881 (2018).
45. Bernkop-Schnürch, A. Strategies to overcome the polycation dilemma in drug delivery. *Adv. Drug Deliv. Rev.* **136**, 62–72 (2018).
46. Smith, S. N. et al. The SHREAD gene therapy platform for paracrine delivery improves tumor localization and intratumoral effects of a clinical antibody. *Proc. Natl Acad. Sci. USA* **118**, e2017925118 (2021).
47. Münch, R. C. et al. Off-target-free gene delivery by affinity-purified receptor-targeted viral vectors. *Nat. Commun.* **6**, 6246 (2015).
48. Zhang, Y. N., Poon, W., Tavares, A. J., McGilvray, I. D. & Chan, W. C. W. Nanoparticle–liver interactions: cellular uptake and hepatobiliary elimination. *J. Control. Release* **240**, 332–348 (2016).
49. Koeberl, D. et al. Interim analyses of a first-in-human phase 1/2 mRNA trial for propionic acidaemia. *Nature* **628**, 872–877 (2024).
50. Sun, Y. et al. In vivo editing of lung stem cells for durable gene correction in mice. *Science* **384**, 1196–1202 (2024).
51. Dilliard, S. A., Cheng, Q. & Siegwart, D. J. On the mechanism of tissue-specific mRNA delivery by selective organ targeting nanoparticles. *Proc. Natl Acad. Sci. USA* **118**, e2109256118 (2021).
52. Yousefi, Z. et al. An update on human papilloma virus vaccines: history, types, protection, and efficacy. *Front. Immunol.* **12**, 805695 (2022).
53. Werness, B. A., Levine, A. J. & Howley, P. M. Association of human papillomavirus types 16 and 18 E6 proteins with p53. *Science* **248**, 76–79 (1990).
54. Ansari, T., Brimer, N. & Vande Pol, S. B. Peptide interactions stabilize and restructure human papillomavirus type 16 E6 to interact with p53. *J. Virol.* **86**, 11386–11391 (2012).
55. Moussa, E. M. et al. Immunogenicity of therapeutic protein aggregates. *J. Pharm. Sci.* **105**, 417–430 (2016).
56. Baird, R. D. et al. First-in-human phase i study of MP0250, a first-in-class DARPin drug candidate targeting VEGF and HGF, in patients with advanced solid tumors. *J. Clin. Oncol.* **39**, 145–154 (2021).

Methods

Selection and screening of DARPin binders specific for the p53 DBD

To generate DARPin binders, *Escherichia coli* expression plasmids of *E. coli* biotin ligase BirA and p53 DBD-OD (amino acids 94–363 of full-length p53; amino acids 94–294 correspond to the DBD and amino acids 325–355 corresponding to the oligomerization domain (OD)) containing an Avi-tag were cotransformed in BL21 (DE3) Rosetta cells (Structural Genomics Consortium Frankfurt) for protein production and in vivo biotinylation. The cells were grown in 2xYT medium supplemented with 100 µM $ZnCl_2$ and 10 µM biotin to an OD of 0.8. Protein expression was induced with 0.6 mM isopropyl β-D-1-thiogalactopyranoside (IPTG) for 16 h at 16 °C. The cells were collected by centrifugation, resuspended in immobilized metal ion affinity chromatography (IMAC) A buffer (50 mM HEPES buffer, pH 7.4, 400 mM NaCl, 20 mM β-mercaptoethanol and 10 µM $ZnCl_2$) supplemented with DNAse (Sigma), RNAse (Sigma) and self-made protease inhibitors (protease inhibitor cocktail (100×): 250 mM 4-(2-aminoethyl)benzenesulfonyl fluoride hydrochloride (AEBSF), 25 mM leupeptin, 25 mM bestatin, 0.75 mM aprotinin, 12.5 mM E-64 and 2.5 mM pepstatin A dissolved in 50% methanol at 4 °C; the solvent was evaporated under vacuum and stored at −20 °C; before use, the protease inhibitor cocktail pellet was resuspended in 1 ml Milli-Q H_2O or buffer; all chemicals were bought from Carl Roth GmbH) and lysed by sonication. The lysate was cleared by centrifugation at 4 °C, the supernatant was supplemented with 30 mM imidazole and applied onto a pre-equilibrated IMAC column (HiTrap IMAC Sepharose FF, Cytiva). The bound protein was washed with IMAC A buffer supplemented with 50 mM imidazole and eluted by a step gradient with IMAC A buffer supplemented with 300 mM imidazole. The eluted protein was then simultaneously dialyzed to IMAC A buffer and digested with a tobacco etch virus (TEV) protease. After the dialysis step, heparin affinity chromatography (HAC) was performed to separate the p53 DBD-OD from any impurities. Before loading the protein solution on a HiTrap heparin HP column (Cytiva), the protein solution was diluted 1:8 in HAC buffer A (25 mM HEPES pH 7.4 and 0.5 mM tris(2-carboxyethyl)phosphine (TCEP)). Bound protein was eluted by applying an increasing gradient of HAC buffer B (25 mM HEPES pH 7.4, 1000 mM NaCl and 0.5 mM TCEP) using an AKTA purifier system at 4 °C. The central peak fractions were pooled, concentrated and loaded onto a HiLoad Superdex 75 16/600 column (Cytiva) using an AKTA purifier system at 4 °C. The purity and molecular weight of the purified proteins were monitored by SDS–polyacrylamide gel electrophoresis (SDS–PAGE) and liquid chromatography–electrospray ionization and time-of-flight mass spectrometry (LC–ESI-TOF-MS).

The biotinylated p53 (amino acids 94–363) containing the DBD and OD domains was immobilized on either MyOne T1 streptavidin-coated beads (Pierce) or Sera-Mag neutravidin-coated beads (GE Healthcare), depending on the particular selection round, and these beads were alternated. The ribosome display selections were performed essentially as described[23] but using a semiautomatic KingFisher Flex MTP 96-well platform.

The library included N3C-DARPins with the original randomization strategy as reported[30] but used a stabilized C-cap[21,57,58]. Additionally, the library was a mixture of DARPins with randomized and non-randomized N- and C-terminal caps, respectively[21,59]. Successively enriched pools were cloned as intermediates in a ribosome display-specific vector[59]. The selections were performed over four rounds with decreasing target concentration and increasing washing steps to enrich for binders with high affinities. In addition, a prepanning with bovine serum albumin (BSA)-blocked streptavidin-coated or neutravidin-coated beads was performed to eliminate unspecific DARPins in rounds 2–4.

DARPin screening

The final enriched pool was cloned as fusion construct into a bacterial pQE30 derivative vector with an N-terminal MRGS(H)8 tag and a C-terminal FLAG tag via unique BamHI × HindIII sites containing a *T5lac* promoter and *lacIq* for expression control.

After transformation of *E. coli* XL1-blue, 380 single DARPin clones for p53 (amino acids 94–363) were expressed in 1 ml scale in deep-well plates by addition of IPTG, and the cells were collected by centrifugation and lysed by addition of B-Per Direct detergent plus lysozyme and nuclease (Pierce). The lysates were cleared by centrifugation. These bacterial crude extracts of single DARPin clones were subsequently used in a HTRF-based screen to identify potential binders. Binding of the FLAG-tagged DARPins to streptavidin-immobilized biotinylated p53 (amino acids 94–363) was measured using fluorescence resonance energy transfer (FRET) (donor: streptavidin-Tb cryptate (610SATLB, Cisbio), acceptor: mAb anti-FLAG M2-d2 (61FG2DLB, Cisbio). Further HTRF measurement against 'no target' allowed for discrimination of p53 (amino acids 94–363)-specific hits. Additionally, p53 DBD-specific hits were confirmed by using biotinylated p53 DBD (amino acids 94–294) lacking the OD. The experiments were performed at room temperature in white 384-well Optiplate plates (PerkinElmer) using the Taglite assay buffer (Cisbio) at a final volume of 20 µl per well. FRET signals were recorded after an incubation time of 30 min using a Varioskan LUX Multimode Microplate (Thermo Scientific). The HTRF ratios were obtained by dividing the acceptor signal (665 nm) by the donor signal (620 nm) and multiplying this value by 10,000 to derive the 665/620 ratio. The background signal was determined by using reagents in the absence of DARPins.

Characterization of purified DARPins

From the identified binders, 32 clones binding to both p53 DBD-containing targets were sequenced, and the single clones were identified. For the selection of p53 DBD-specific DARPins, 23 DARPins were unique, and the single clones were expressed on a 1 ml scale. The cells were lysed using a cell lytic B reagent (Sigma), lysozyme and Pierce nuclease and purified using a 96-well IMAC column (HisPur Cobalt plates, Thermo Scientific). The DARPins after IMAC purification were analyzed at a concentration of 10 µM on a Superdex 75 5/150 GL column (GE Healthcare) using an Akta Micro system (GE Healthcare) with PBS containing 400 mM NaCl as the running buffer. Out of the panel of 23 p53 DBD-binding DARPins, 3 were chosen for further analysis: DARPin C10 (006-627-1801-C10), DARPin B12 (006-627-1803-B12) and DARPin F12 (006-627-1804-F12).

Cell culture

HeLa, SiHa and U-2 OS cell lines were cultured in DMEM medium (Gibco) supplemented with 10% fetal bovine serum (FBS, Capricorn Scientific), 1 mM pyruvate (Gibco), 100 U ml^{-1} penicillin (Gibco) and 100 µg ml^{-1} streptomycin (Gibco) at 37 °C and 5% CO_2. The HeLa cells were obtained from CLS Cell Lines Service GmbH. The U-2 OS cells were a gift from Prof. Dr. Ivan Đikić (IBCII, Goethe University, Frankfurt am Main). The SiHa cells were obtained from Biozol. T-REx HeLa and T-REx U-2 OS cell lines were obtained from Christian Behrends (Munich Cluster for Systems Neurology (SyNergy) and Ludwig-Maximilians-University) and were cultured in DMEM medium (Gibco), containing 10% FBS (Capricorn Scientific), 4 µg ml^{-1} blasticidin (Gibco), 333 µg ml^{-1} Zeocin (Gibco), 100 U ml^{-1} penicillin (Gibco), 100 µg ml^{-1} streptomycin (Gibco) and 1 mM pyruvate (Gibco) at 37 °C and 5% CO_2. The cell lines used in this study were frequently tested for mycoplasma contaminations.

For recombinant protein expression, the cells in DMEM without antibiotics were transfected using Lipofectamine 2000 as transfection reagent according to the manufacturer's recommendations. A total of 6 h after transfection, the medium was exchanged to standard culturing medium with antibiotics.

Generation of stable cell lines expressing DARPin C10 or control DARPin

The HeLa and U-2 OS cell lines stable expressing DARPin C10 or the control DARPin E3_5 were generated using the Flp-In T-Rex system (Thermo

Fisher Scientific) for homologous recombination. After 2 weeks of culturing T-REx HeLa or T-Rex U-2 OS cells, they were transfected with pcDNA5/FRT/TO (Thermo Fisher Scientific) containing the respective DARPin and with pOG44 (Thermo Fisher Scientific) containing the Flp recombinase according to the manufacturer's recommendations. After transfection, the medium was exchanged to DMEM supplemented with 10% tetracycline-free FBS (BioCell). The next day after transfection, the cells were reseeded in 15 cm dishes, and 24 h after cell transfer, the medium was exchanged to the selection medium (DMEM supplemented with 10% tetracycline-free FBS, 4 μg ml^{-1} blasticidin, 200 μg ml^{-1} hygromycin (Thermo Fisher Scientific), 100 U ml^{-1} penicillin, 100 μg ml^{-1} streptomycin and 1 mM pyruvate. The cells were cultured for 10–14 days until a non-transfected control showed no viable cells. Six single colonies of each cell line were isolated and cultured, and inducible expression of the desired protein was tested by fluorescence staining. The protein expression was induced by adding 1 μg ml^{-1} tetracycline (Thermo Fischer Scientific) to the selection medium for 24 h.

The SiHa cell lines stably expressing DARPin C10 or control DARPins were generated using the PiggyBac Transposon system (System Biosciences) according to the manufacturer's instructions. In brief, the cells were transfected with 200 ng PiggyBac Transposase vector (PB210PA-1, System Biosciences) and 500 ng PB Cumate switch Transposon vector (PBQM812A-1) containing the respective DARPins. A total of 6 h after transfection, the cells were split into multiple wells of a six-well plate and grown to confluency. Puromycin selection (2.5 μg ml^{-1}) was applied for 3–5 days to establish positively transposed cells. The inducible expression of the desired protein was tested by fluorescence staining using an anti-Myc antibody to detect the tag of the DARPin. Expression was induced by addition of 30 μg ml^{-1} Cumate (PBQM100-A, System Biosciences) to the medium for 24 h.

Molecular cloning

For recombinant protein expression of DARPins, HPV E6 and all DBD constructs, a pET-15b vector (Novagen, Merck KGaA) was used. The inserts generated by PCR were introduced into pET-15b-His_{10}-TEV (N-terminal His_{10}-tag followed by a TEV protease cleavage site), pET-15b-His_{10}-TEV-Avi (N-terminal His_{10}-tag followed by a TEV protease cleavage site and Avi-tag), pET-15b–GFP-His_8-TEV (N-terminal GFP followed by a His_8-tag and a TEV protease cleavage side) or pGEX-6P-2-His_8-TEV (N-terminal GST-tag followed by His_8-tag and TEV protease cleavage site) by subcloning using BamHI and XhoI restriction sites. For transient expression in mammalian cells, PCR-generated inserts were introduced into pcDNA3.1(+) Myc (Invitrogen, Thermo Fisher Scientific) by subcloning using BamHI and XhoI restriction sites. The H82R mutation in the optimized DARPin C10 variant was introduced by site-directed mutagenesis PCR using primers containing the mutated codon.

Protein expression and purification

DARPins. DARPins were expressed in *E. coli* and purified as described before[24,25]. In brief, the respective pET-15b expression plasmid was transformed into *E. coli* BL21(DE3) Rosetta cells. The cells were grown in 2xYT medium until an optical density of 0.8 was reached. The protein expression was induced with 0.6 mM IPTG for 16 h at 16 °C. The cells were collected by centrifugation, resuspended in IMAC A buffer (50 mM HEPES pH 7.2 and 400 mM NaCl) supplemented with RNAse (Sigma), DNAse (Sigma), lysozyme (Sigma) and self-made protease inhibitors and were lysed by sonification. After clearing the lysate by centrifugation, the supernatant was supplemented with 30 mM imidazole and loaded on a pre-equilibrated IMAC column (HiTrap IMAC Sepharose FF, Cytiva), following an IMAC purification protocol. The bound protein was washed with IMAC A buffer supplemented with 50 mM imidazole and eluted by a step gradient with IMAC A buffer supplemented with 300 mM imidazole. The eluted protein was simultaneously dialyzed to IMAC A buffer and digested with TEV protease (self-made). The TEV protease and undigested protein were separated by a reverse IMAC step. The purified proteins were further purified and buffer-exchanged by size-exclusion chromatography (SEC) with SEC buffer (50 mM Tris, pH 8, 150 mM NaCl and 0.5 mM TCEP) using a Superdex 75 10/300 column (Cytiva) on an AKTA purifier system at 4 °C. The central peak fractions were collected, concentrated to a concentration of 300–500 μM (Amicon Ultra Centrifugal Filters, Millipore) and flash frozen in liquid nitrogen before storage at −80 °C until use. The purity and molecular weight of purified proteins was monitored by SDS–PAGE and LC–ESI-TOF-MS.

p53 DBD and HPV E6 protein. The pET-15b-derived expression plasmids were transformed and expressed in *E. coli* BL21(DE3) Rosetta cells as described before[24]. HPV E6 proteins were expressed either as GFP or as GST-fusion proteins and purified as described for the DARPins. For DBD and E6 proteins, the expression medium was supplemented with 100 μM $ZnCl_2$, and the IMAC buffers were supplemented with 20 mM β-mercaptoethanol and 10 μM $ZnCl_2$. Cell lysis, IMAC, dialysis and TEV-digestion were performed as described for the DARPins. For the p53 DBD, HAC was performed after the dialysis step to separate the p53 DBD from any impurities. Before loading the protein solution on a HiTrap heparin HP column (Cytiva), the protein solution was diluted 1:8 in HAC buffer A (25 mM HEPES pH 7.4 and 0.5 mM TCEP). The bound protein was eluted by applying an increasing gradient of HAC buffer B (25 mM HEPES pH 7.4 and 1,000 mM NaCl 0.5 mM TCEP) using an AKTA purifier system at 4 °C. The central peak fractions were pooled, concentrated and loaded onto a HiLoad Superdex 75 16/600 column (Cytiva) using an AKTA purifier system at 4 °C. The purity and molecular weight of the purified proteins was monitored by SDS–PAGE and LC–ESI-TOF-MS.

DARPin biotinylation

In vitro biotinylation of Avi-tagged DARPins was performed as described previously[24]. In brief, the *E. coli* biotin ligase BirA was subcloned into a pET-15b-GFP-His8-TEV *E. coli* expression vector. GFP–BirA was expressed and purified as described before, except for a TEV cleavage and reverse IMAC step.

DARPins containing an Avi-Tag were enzymatically biotinylated in vitro by mixing them with GFP–BirA in a 1:50 molar ratio in SEC buffer supplemented with 10 mM ATP, 10 mM $MgCl_2$ and 0.5 mM biotin, followed by 16 h incubation at 16 °C. For separation, the reaction mix was applied onto a Superdex 75 10/300 column (Cytiva). DARPin fractions were pooled and analyzed by LC–ESI-TOF-MS. Only DARPins showing 100% labeling efficacy were used for experiments.

Pulldown assays

DARPin pulldown assays. The recombinant target proteins were expressed in H1299 cells, and respective cell lysates were generated as described before[24]. Biotinylated DARPins were immobilized on pre-equilibrated magnetic Dynabeads MyOne Streptavidin T1 (Thermo Fisher Scientific) in pulldown wash buffer (50 mM Tris pH 8, 150 mM NaCl, 0.1% (v/v) Tween-20), rotating for 2 h at 4 °C. Unbound DARPin was removed by washing three times with pulldown wash buffer, and the beads were resuspended in the same volume of PD wash buffer as before to maintain the bead concentration. Per sample, 10 μl DARPin-loaded beads were mixed with cell lysate, 1× complete protease inhibitor (Roche), and the total volume was adjusted to 1,000 μl with pulldown wash buffer. The samples were incubated by rotating overnight at 4 °C. The next day, the beads were washed five times with 1,000 μl pulldown wash buffer, and the bound proteins were eluted by incubating with lithium dodecyl sulfate (LDS) buffer at 70 °C for 10 min. The samples were analyzed by western blot as described before. All pulldown experiments in this study were performed as biological triplicates unless stated otherwise.

Competitive pulldown of HPV E6. Avi-tagged p53 DBD (amino acids 94–294) was expressed in *E. coli* and purified as described above followed by in vitro biotinylation. An excess of biotinylated p53 DBD was incubated by rotating with Dynabeads MyOne Streptavidin T1 (Thermo Fisher Scientific) for 1 h at 4 °C, and the unbound protein was removed by washing three times with pulldown wash buffer. Per sample, 10 µl preloaded beads, 10 µM GFP-fused HPV E6 protein, 10 µM maltose binding protein-fused E6AP peptide (described in[13]), 15 µM DARPin and 1× complete protease inhibitor (Roche) were mixed, and the total volume was adjusted to 1,000 µl with pulldown wash buffer. The samples were incubated rotating overnight at 4 °C. The next day, the beads were washed five times with 1,000 µl pulldown wash buffer, and the bound proteins were eluted with LDS buffer boiling at 70 °C for 10 min. The samples were analyzed by western blot as described before. GFP-fused E6 protein was detected using an anti-GFP antibody. The pulldown was performed in triplicates, and the signals were quantified using ImageLab (version 6.1, Bio-Rad).

ITC

All titration experiments were performed using a MicroCal VP-ITC microcalorimeter (Malvern Instruments). DARPins and p53 family DBDs were dialyzed against the ITC buffer (50 mM HEPES pH 7.4, 150 mM NaCl and 0.5 mM TCEP). The DBDs were titrated to constant concentrations of DARPin in 25 injections of 10 µl each, with a spacing time of 250 s and a stirring speed of 307 r.p.m. The measurements were performed at 15 °C or 25 °C, with the reference power set to 25 µcal s^{-1}. NITPIC was used for unbiased baseline calculation and curve integration[60]. The thermodynamic parameters and final binding affinities were calculated using SEDPHAT, assuming an AB heteroassociation model[61] and are listed in Supplementary Table 1. The first data point was excluded from the analysis. The final figures were generated using GUSSI[62].

Protein crystallization and structure determination

The protein complexes for crystallization were prepared by mixing DARPin C10 or C10-H82R and the p53 DBD at a 1:1 molar ratio in SEC buffer, each at 60 µM protein concentration. The protein mix was incubated overnight at 4 °C, and the formed complex was separated from unbound proteins by SEC using a Superdex 75 10/300 column. The central peak fractions corresponding to the protein complex were pooled, concentrated to 2.5–2.6 mg ml^{-1} and analyzed by SDS–PAGE as well as LC–ESI-TOF-MS. The crystals were grown at 293 K using the sitting drop vapor diffusion technique with a mosquito crystallization robot (TTP Labtech). The protein solution was mixed with reservoir solution (25% w/v polyethylene glycol 3350 for C10; 0.1 M Bis–Tris propane, pH 7.5, 0.02 M sodium potassium phosphate, pH 7.5, 20% (w/v) polyethylene glycol 3350 and 10% (v/v) ethylene glycol for C10-H82R) at a 2:1 ratio (final drop volume 200 nl). The crystals were cryoprotected with mother liquor supplemented with 23% ethylene glycol and flash frozen in liquid nitrogen. X-ray diffraction data sets were collected at 100 K at beamline X06SA of the Swiss Light Source. The diffraction data were integrated with the program XDS[63] and scaled with AIMLESS[64], which is part of the CCP4 package[65]. The structure of the p53-DARPin C10 complex was then solved by molecular replacement with PHASER[66] using structures of the p53 DBD (PDB entry 2XWR)[67] and DARPin 8F1 (PDB entry 7Z73)[24] as search models. Model building and refinement was then performed using iterative cycles of manual model building in COOT[68] and refinement in PHENIX[69]. For the C10-H82R mutant, the structure was solved by Fourier synthesis in Phenix with the structure of the C10 complex as a starting model and subsequently refined as described for the C10 complex. Validation of the final models was performed using MolProbity[70]. For both structures, 99.7% of the residues were in the favored regions of the Ramachandran plot, and there were no outliers. X-ray data collection and refinement statistics are listed in Table 1. The interface areas were calculated using the PISA server (http://www.ebi.ac.uk/pdbe/prot_int/pistart.html)[71] and are defined as the difference in total accessible surface areas of isolated and interfacing structures divided by two. The structural figures in this paper were prepared with PyMOL (www.pymol.org).

Gel electrophoresis and western blotting

The purified proteins were mixed with SDS loading buffer (250 mM Tris, pH 8.0, 7.5% (w/v) SDS, 25% (w/v) glycerol, 12.5% (v/v) β-mercaptoethanol and 0.025% (w/v) bromophenol blue), denatured at 95 °C and separated on manually prepared discontinuous 4–16% Tris–glycine gels. The gels were subsequently stained using Quick Coomassie Stain (NeoBiotech) according to the manufacturer's recommendations.

The samples for immunoblotting were either mixed with SDS loading buffer or NuPAGE LDS buffer (Thermo Fisher Scientific) supplemented with dithiothreitol, denatured at 95 °C and applied on 4–15% Mini-PROTEAN TGX Stain-Free Precast Protein gels (Bio-Rad). The gels were transferred using the TransBlot Turbo Transfer System (Bio-Rad) according to the manufacturer's recommendations. The membranes were blocked for 1 h in blocking buffer (TBS, 0.05% (v/v) Tween-20, 5% skim milk powder, Sigma-Aldrich) and incubated with primary antibody in blocking buffer overnight shaking at 4 °C. The membranes were washed three times with Tris-buffered saline with 0.1% (v/v) Tween-20 (TBS-T), followed by incubation with secondary antibody in blocking buffer under shaking for 1 h at room temperature. Afterward, membranes were washed three times with TBS-T and analyzed by adding Amersham ECL Prime WB Detection Reagent (Cytiva). The quantification of western blot signals was performed using ImageLab (version 6.1, Bio-Rad). Vinculin was used as loading control as the band of vinculin does not overlap with p53. Therefore, both proteins can be detected on the same blot.

The following antibodies and dilutions were used: anti-Myc (1:2,000, clone 4A6, Millipore), anti-p53 (1:500, DO-I, Santa Cruz Biotechnology), anti-vinculin (1:2,000, clone 7F9, Santa Cruz Biotechnology) and goat anti-mouse IgG (Fab-specific)-peroxidase conjugate (1:5,000, A9917, Sigma-Aldrich).

HPV p53 degradation assay

Full-length TAp53α was in vitro translated using the TNT T7 Quick coupled Transcription/Translation system (Promega). For in vitro translation, pcDNA3.1(+) containing the TAp53α gene was diluted to 100 ng $µl^{-1}$, mixed with RRL in a 1:4 ratio and incubated at 30 °C for 90 min. The reaction was stopped by addition of benzonase (Millipore) for 30 min. Afterward, 22.5 µl RRL were mixed with 2 µM GST or GST-E6 and 10 µM DARPin. The sample volume was adjusted to 60 µl with 2× reaction buffer (50 mM Tris pH 7.5, 200 mM NaCl and 4 mM dithiothreitol). The reaction mix was then incubated at 25 °C, and the samples were taken at different time points by mixing 5 µl reaction mix with 25 µl 5× SDS sample buffer and boiling at 95 °C for 1 min. Degradation of p53 was analyzed by western blot using an α-Myc antibody. The degradation assay was performed in biological triplicates.

Transactivation assay

For transactivation assays, HeLa, U-2 OS or SiHa cells were seeded in 12-well plates and transfected using Lipofectamine 2000 as transfection reagent (Thermo Fisher Scientific) according to the manufacturer's instructions. All transfection mixes included 200 ng of pRL-CMV (Promega) for constitutive expression of *Renilla* luciferase, 200 ng of a reporter plasmid with firefly luciferase under the control of a specific promotor and varying amounts of pcDNA3.1(+) with the respective DARPin. For each assay, an empty vector control comprising only empty pcDNA3.1(+) was transfected to determine the fold induction without presence of any DARPin. A total of 24 h after transfection, the cells were washed with PBS (Gibco), detached with Accutase and reseeded into white Nunc 96-well microplates (Thermo Fisher scientific) in quadruplicates. The assay was performed using the Dual-Glo luciferase reporter assay kit (Promega) according to the manufacturer's instructions, and

firefly as well as *Renilla* luciferase fluorescence was measured using a Spark plate reader (Tecan). The remaining sample was centrifuged for 5 min at 500*g*, the pelleted cells were mixed with 1× SDS loading buffer and the p53 protein levels were analyzed by western blot using the anti-p53 (DO-I) antibody (Santa Cruz Biotechnology). The experiment was repeated in three biological replicates, and the ratio of firefly to *Renilla* luciferase signal was normalized to empty vector control for each biological replicate. The statistical significance was assessed by ordinary one-way analysis of variance (ANOVA) (not significant (n.s.), $P > 0.05$; $^{*}P \leq 0.05$, $^{**}P \leq 0.01$, $^{***}P \leq 0.001$, $^{****}P \leq 0.0001$) using Prism (Version 8.2.1, GraphPad).

qPCR

For qPCR analysis of the expression of p53 target genes, HeLa, U-2 OS or SiHa cells were transfected with pcDNA3.1(+) plasmids containing the respective DARPin using Lipofectamine 2000 as transfection reagent (Thermo Fisher Scientific) according to the manufacturer's instructions. A total of 24 h after transfection, the cells were washed with PBS, detached and mRNA was isolated using the RNease mini kit (Qiagen). Reverse transcription of mRNA was performed using the SuperScript IV VILO Master Mix with the ezDNase-enzyme kit (Thermo Fisher Scientific). Both kits were used according to the manufacturer's instructions. qPCR was performed in technical triplicates using the TaqMan fast advanced Master Mix and the respective TaqMan Assay (Thermo Fisher Scientific) using a QuantStudio 5 Real Time PCR system (Thermo Fisher Scientitic). The target gene expression was referenced to the housekeeping gene HPRT-1. The experiment was repeated in three biological replicates, and the statistical significance was assessed by ordinary one-way ANOVA (n.s., $P > 0.05$; $^{*}P \leq 0.05$, $^{**}P \leq 0.01$, $^{***}P \leq 0.001$, $^{****}P \leq 0.0001$) using Prism (Version 8.2.1, GraphPad).

Preparation of mRNA by in vitro transcription

For in vitro transcription, PCR-generated inserts of DARPin C10, control DARPin and GFP were introduced into a modified pcDNA3.1 plasmid in which the 5′ untranslated region (UTR) of human β-globin was introduced between the T7 promotor and the DARPin insert using NheI and HindIII. Additionally, the 3′ UTR of human β-globin followed by a 120-bp poly(A) tail was cloned behind the DARPin insert using KpnI and SpeI. The plasmids were linearized using SpeI and in vitro transcribed using the HiScribe T7 ARCA mRNA Kit (New England Biolabs) with the modified nucleotides pseudo-UTP and 5′-methyl-CTP according to the manufacturer's instructions. RNA was purified using the RNeasy mini kit (Qiagen). The RNA concentration was determined by measuring the absorption at 260 nm, and the RNA quality was confirmed by running a 1% agarose gel.

mRNA transfection

The cells were transfected with the respective mRNA using Lipofectamine MessengerMax (Invitrogen) according to the manufacturer's instructions. RNA isolation, reverse transcription and qPCR were performed as described above.

siRNA transfection

The cells were transfected with the respective siRNA using Dharmafect 1 transfection agent (Dharmacon) according to the manufacturer's instructions. As a negative control the ON-TARGETplus Non-Targeting Pool siRNA (Dharmacon) was used. The siRNA for knockdown of HPV16 E6 was ordered from Santa Cruz biotechnology, and the siRNA for knockdown of HPV18 E6 was designed on the basis of the sequence published previously[72] and ordered from Dharmacon.

IF staining

A total of 24 h after transfection or induction of protein expression, the cells were washed twice with PBS and fixed with PFA for 10 min at room temperature. The fixed cells were washed twice with PBS and permeabilized with PBS-T (PBS supplemented with 0.1% Triton X-100) for 5 min two times. The permeabilized cells were blocked with blocking buffer (PBS-T supplemented with 1% BSA) for 20 min at room temperature. The blocked cells were incubated with rabbit anti-Myc (1:500, Abcam ab9106) and mouse anti-p53 (1:250, DO-I, Santa Cruz) antibodies in blocking buffer overnight at 4 °C. The cells were washed three times with PBS-T and incubated with Alexa Fluor 568 anti-rabbit (1:200, A10042, Life Technologies) and Alexa Fluor 647 anti-mouse antibody (1:200, A31571, Life Technologies) in blocking buffer for 2 h at room temperature. The slides were washed three times with PBS-T and mounted using Mowiol (Carl Roth) mounting medium, which was supplemented with 4,6-diamidino-2-phenylindole (Thermo Fisher Scientific). The detailed recipes of the mounting medium can be found at CSH Protocols (http://cshprotocols.cshlp.org/content/2006/1/pdb.rec10255). The slides were dried for at least 1 day before imaging with an LSM 780 confocal laser scanning microscope (Zeiss).

RNA-seq

RNA was isolated using the RNeasy Mini Kit (QIAGEN, 74106) according to the manufacturer's protocol. The RNA quality assessment was performed using the Experion RNA StdSens Analysis Kit (Bio-Rad, 700-7103). The RNA-seq libraries were prepared from total RNA with the Lexogen QuantSeq 3′-mRNA Library Prep Kit FWD for Illumina (Lexogen, 015.24) in combination with the UMI Second Strand Synthesis Module for QuantSeq FWD (Illumina, Read 1) (Lexogen, 081.96) following the manufacturer's protocol. The sequencing library quality was checked on a Bioanalyzer 2100 using the Agilent High Sensitivity DNA Kit. The pooled sequencing libraries were quantified and sequenced on the NextSeq 550 platform (Illumina) with 75-base single reads.

After sequencing, unique molecular identifiers (UMIs) were extracted from the obtained FASTQ files for sequenced reads, and the QuantSeq FWD-UMI 3′ spacer corresponding to the first four nucleotides was removed. The trimmed reads were then aligned to the *Homo sapiens* Ensembl reference genome (revision 109, GRCh38), using the STAR RNA-seq aligner (version 2.7.10a)[73]. Subsequently, UMI deduplication was done via UMI-tools (version 1.1.2)[74]. UMIs per gene were quantified and normalized to counts per million, and threshold filtering was applied to exclude genes with a counts per million <1 in all samples. Pair-wise comparisons were performed, and differential expression was determined using DEseq2 (version 1.36.0)[75]. The false discovery rate (FDR) was controlled via Benjamini–Hochberg corrected *P* values ($\alpha = 0.05$). The genes showing a $\log_2$ fold change ($\log_2$FC) ≥1, and the corrected *P* values <0.05 were considered differentially expressed. The volcano plots and bar charts were generated using the matplotlib library (version 3.6.2). GSEA was performed using the GSEA software (version 4.3.2)[76] and Molecular Signatures Database (MSigDB, version 7.1). The reported FDR is the ratio of the actual enrichment score versus the scores of all gene sets for all permutations and the actual enrichment score versus the score of all gene sets in the actual unpermutated data set. The nominal *P* value is unadjusted for multiple hypothesis testing or gene set size, while the FDR is adjusted for both.

Cell survival assays

T-Rex HeLa cells, T-Rex U-2 OS cells or SiHa cells stably expressing DARPin C10 or control DARPin were seeded into white Nunc 96-well microplates (Thermo Fisher Scientific), and protein expression was induced as described before. A total of 24 h after induction, the medium was exchanged to medium containing substrate and NanoLuc enzyme according to the manufacturer's instructions using the RealTime-Glo MT assay kit (Promega). The luminescence was monitored continuously using a Spark plate reader (Tecan).

For detection of apoptosis induction and cell death, HeLa and SiHa cells were transfected with mRNA encoding the control DARPin,

DARPin C10 or DARPin C10-H82R. A total of 48 h after transfection, the membrane integrity as a marker of cell death was detected using the CellTox Green Cytotoxicity Assay (Promega) according to the manufacturer's instructions. Caspase 3 and 7 activity as a marker of apoptosis induction was detected using the Caspase Glo 3/7 Assay (Promega).

Statistics and reproducibility

Pulldown experiments, p53 degradation assays, transactivation assays and qPCR experiments were performed in biological triplicates, and all individual data points are shown in the corresponding figures. The bar diagrams present the mean value and the error bar the standard deviation (s.d.). ITC measurements were performed twice; however, the determination of the K_d values was based on a single measurement. The K_d values and the 95% confidence interval were determined by SEDPHAT. The cell survival assays were performed in triplicates. Each data point presents the mean value and the error bar the s.d. The statistical significance was assessed by ordinary one-way ANOVA (n.s., $P > 0.05$; $^{*}P \leq 0.05$, $^{**}P \leq 0.01$, $^{***}P \leq 0.001$, $^{****}P \leq 0.0001$).

In all quantifications, the data distribution was assumed to be normal but this was not formally tested. No data points were excluded.

Reporting summary

Further information on research design is available in the Nature Portfolio Reporting Summary linked to this article.

Data availability

The atomic coordinates and structure factors of the p53 DBD complexes with DARPin C10 and C10-H82R have been deposited in the Protein Data Bank (PDB) under accession codes 8RCI and 9FZB, respectively. RNA-seq data were deposited at EBI ArrayExpress, accession number E-MTAB-13602. Source data are provided with this paper.

References

57. Kramer, M. A., Wetzel, S. K., Plückthun, A., Mittl, P. R. E. & Grütter, M. G. Structural determinants for improved stability of designed ankyrin repeat proteins with a redesigned C-capping module. *J. Mol. Biol.* **404**, 381–391 (2010).
58. Brauchle, M. et al. Protein interference applications in cellular and developmental biology using DARPins that recognize GFP and mCherry. *Biol. Open* **3**, 1252–1261 (2014).
59. Schilling, J., Schoppe, J. & Pluckthun, A. From DARPins to LoopDARPins: novel LoopDARPin design allows the selection of low picomolar binders in a single round of ribosome display. *J. Mol. Biol.* **426**, 691–721 (2014).
60. Keller, S. et al. High-precision isothermal titration calorimetry with automated peak-shape analysis. *Anal. Chem.* **84**, 5066–5073 (2012).
61. Houtman, J. C. D. et al. Studying multisite binary and ternary protein interactions by global analysis of isothermal titration calorimetry data in SEDPHAT: application to adaptor protein complexes in cell signaling. *Protein Sci.* **16**, 30–42 (2007).
62. Brautigam, C. A. Calculations and publication-quality illustrations for analytical ultracentrifugation data. *Methods Enzymol.* **562**, 109–133 (2015).
63. Kabsch, W. Xds. *Acta Crystallogr. D* **66**, 125–132 (2010).
64. Evans, P. R. An introduction to data reduction: space-group determination, scaling and intensity statistics. *Acta Crystallogr. D* **67**, 282–292 (2011).
65. Winn, M. D. et al. Overview of the CCP4 suite and current developments. *Acta Crystallogr. D* **67**, 235–242 (2011).
66. Mccoy, A. J. et al. Phaser crystallographic software. *J. Appl. Crystallogr.* **40**, 658–674 (2007).
67. Natan, E. et al. Interaction of the p53 DNA-binding domain with its n-terminal extension modulates the stability of the p53 tetramer. *J. Mol. Biol.* **409**, 358–368 (2011).
68. Emsley, P., Lohkamp, B., Scott, W. G. & Cowtan, K. Features and development of Coot. *Acta Crystallogr. D* **66**, 486–501 (2010).
69. Liebschner, D. et al. Macromolecular structure determination using X-rays, neutrons and electrons: recent developments. *Acta Crystallogr. D* **75**, 861–877 (2019).
70. Williams, C. J. et al. MolProbity: more and better reference data for improved all-atom structure validation. *Protein Sci.* **27**, 293–315 (2018).
71. Krissinel, E. & Henrick, K. Inference of macromolecular assemblies from crystalline state. *J. Mol. Biol.* **372**, 774–797 (2007).
72. Butz, K. et al. siRNA targeting of the viral E6 oncogene efficiently kills human papillomavirus-positive cancer cells. *Oncogene* **22**, 5938–5945 (2003).
73. Dobin, A. et al. STAR: ultrafast universal RNA-seq aligner. *Bioinformatics* **29**, 15–21 (2013).
74. Smith, T., Heger, A. & Sudbery, I. UMI-tools: modeling sequencing errors in unique molecular identifiers to improve quantification accuracy. *Genome Res* **27**, 491–499 (2017).
75. Love, M. I., Huber, W. & Anders, S. Moderated estimation of fold change and dispersion for RNA-seq data with DESeq2. *Genome Biol.* **15**, 550 (2014).
76. Subramanian, A. et al. Gene set enrichment analysis: a knowledge-based approach for interpreting genome-wide expression profiles. *Proc. Natl Acad. Sci. USA* **102**, 15545–15550 (2005).

Acknowledgements

The research was funded by the German Research Foundation (DFG) (DO 545/16-1 and DO 545/24-1), the Centre for Biomolecular Magnetic Resonance and the Clusterproject ENABLE (funded by the Hessian Ministry for Science and the Arts) to V.D. A.C.J. is funded by German Research Foundation (DFG) grant JO 1473/1-3. S.K. and A.C.J. are supported by the German Cancer Aid (Krebshilfe) grant TACTIC. D.-I.B., S.K. and A.C.J. are grateful for support by the Structural Genomics Consortium, a registered charity (number 1097737) that received funds from Bayer AG, Boehringer Ingelheim, Bristol Myers Squibb, Genentech, Genome Canada through Ontario Genomics Institute, (OGI-196), EU/EFPIA/OICR/McGill/KTH/Diamond Innovative Medicines Initiative 2 Joint Undertaking (EUbOPEN grant 875510), Janssen, Merck KGaA, Pfizer and Takeda. T.S. is funded by the DFG (STI 182/13-1 and STI 182/15-1), Bundesministerium für Bildung und Forschung (German Center for Lung Research, DZL) and Hessisches Ministerium für Wissenschaft und Kunst (LOEWE iCANx). We thank the staff at beamline X06SA of the Swiss Light Source for assistance during data collection. We thank all current and former members of the High-Throughput Binder Selection facility at the Department of Biochemistry of the University of Zurich for their contribution to the establishment of the semiautomated ribosome display that resulted in the generation of the used DARPin binders, especially Thomas Reinberg, Sven Furler, Thamar Looser and Joana Marinho for the selection and screening of these DARPin binders.

Author contributions

P.M., A.S., D.-I.B, J.S.F., M.M., C.O., M.T., B.Y. and B.S. performed the research and analyzed the data. J.V.S and B.D. coordinated the DARPin generation. S.K., A.P., T.S., A.C.J. and V.D. supervised the research.

Competing interests

A.P. is a cofounder and shareholder of Molecular Partners AG, who are commercializing the DARPin technology. The other authors declare no competing interests.

Additional information

Extended data is available for this paper at https://doi.org/10.1038/s41594-024-01456-7.

Supplementary information The online version contains supplementary material available at https://doi.org/10.1038/s41594-024-01456-7.

Correspondence and requests for materials should be addressed to Volker Dötsch.

Peer review information *Nature Structural & Molecular Biology* thanks the anonymous reviewers for their contribution to the peer review of this work. Peer reviewer reports are available. Primary Handling Editor: Sara Osman, in collaboration with the *Nature Structural & Molecular Biology* team.

https://doi.org/10.1038/s41594-024-01456-7

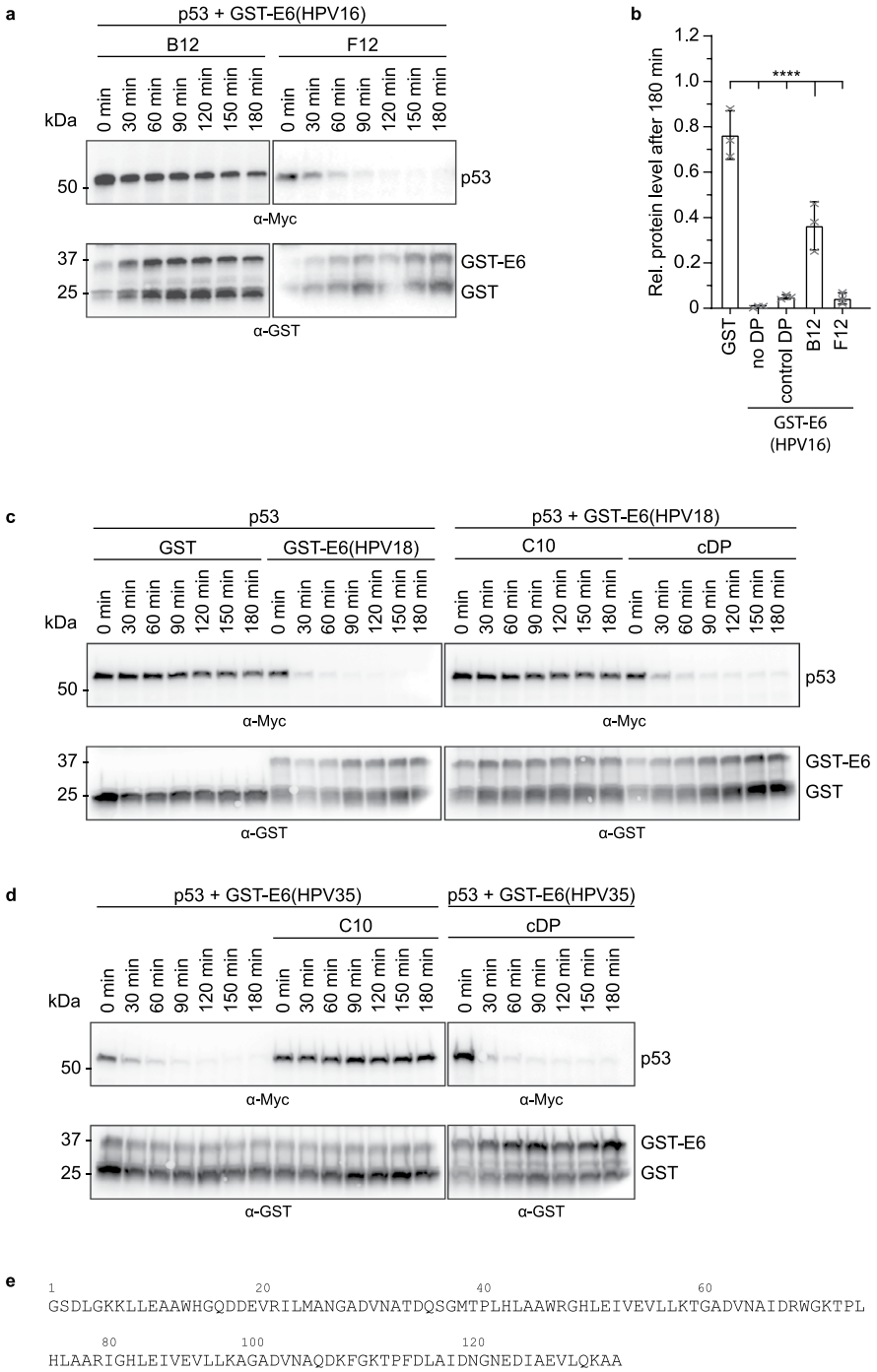

Extended Data Fig. 1 | Effect of DARPins on E6-mediated p53 degradation. **a**, In vitro assay to investigate HPV16-E6 mediated degradation of p53 by various DARPins. The HPV-E6 protein binds to the p53 DBD and recruits the E3-ubiquitin ligase E6AP, leading to ubiquitination and proteasomal degradation of p53. Myc-tagged p53 was in vitro translated in rabbit reticulocyte lysates (RRL) and co-incubated with a GST fusion of the HPV16-E6 protein (GST-E6) with or without the respective DARPin (DP). Samples were analyzed using an α-Myc antibody (upper panel) or an α-GST antibody (lower panel). Co-incubation of p53 with GST did not show any degradation, whereas incubation with GST-E6 led to degradation of p53. Co-incubation of p53 with E6 and DARPin B12 partially prevented the HPV-E6 mediated degradation of p53, whereas the DARPin F12, as an example of a non-inhibitory binder, had no effect. **b**, Quantification of the degradation assay in (**a**), including the non-binding control DARPin. The relative protein level after 180 min normalized to the protein level after 0 min is shown on the y-axis. The bar diagram shows the mean values and the error bars the corresponding SD of three biological replicates. An ordinary one-way ANOVA was performed to assess the statistical significance (n.s.: $P > 0.05$, *: $P \leq 0.05$, **: $P \leq 0.01$, ***: $P \leq 0.001$, ****: $P \leq 0.0001$). **c**, In vitro assay to investigate HPV18-E6 mediated degradation of p53. Myc-tagged p53 was in vitro translated in RRL and co-incubated with a GST fusion of the HPV18-E6 protein (GST-E6) with or without respective DARPin. Samples were analyzed using an α-Myc antibody (upper panel) or an α-GST antibody (lower panel). Co-incubation of p53 with GST did not show any degradation, whereas incubation with GST-E6 led to degradation of p53. Co-incubation of p53 with E6 from HPV18 and DARPin C10 prevented the HPV-E6 mediated degradation of p53 as it did for E6 from HPV16, whereas the control DARPin had no effect. **d**, Same assay as in (**c**) but with HPV35-E6, again showing very similar results as for HPV16. The assays in (**c**) and (**d**) were performed in biological triplicates, with the western blots of one replicate shown. **e**, Amino acid sequence of DARPin C10.

https://doi.org/10.1038/s41594-024-01456-7

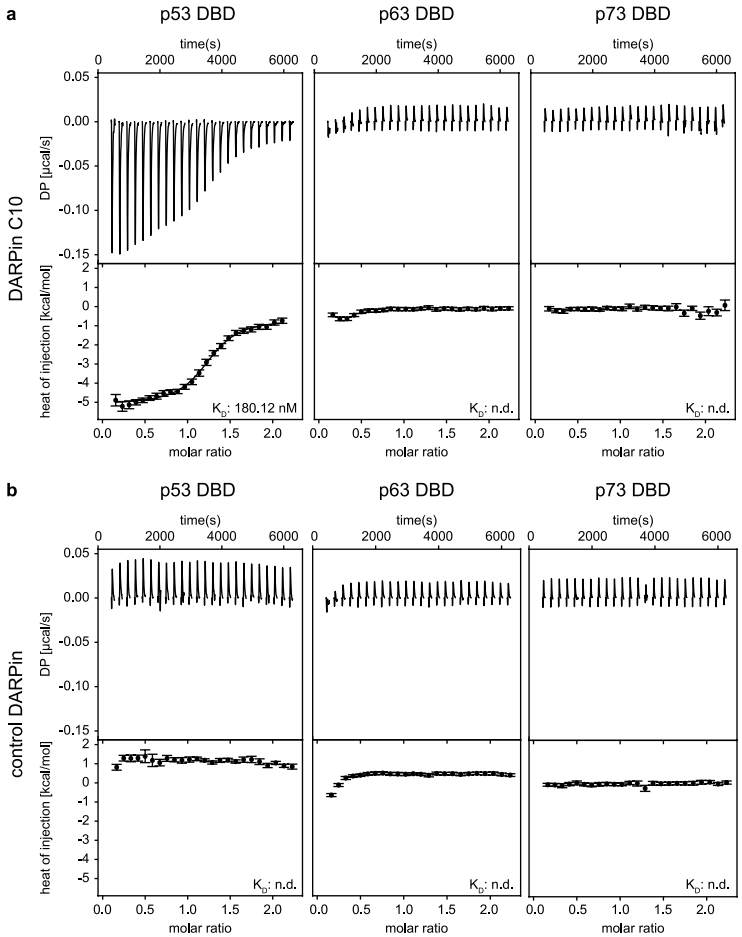

Extended Data Fig. 2 | Binding of DARPin C10 to p53 family members. a, ITC measurements with DARPin C10 and the DNA-binding domains of p53, p63 and p73 performed at 15 °C. The top diagram shows the raw measurement and the bottom diagram the integrated heat per titration step. No interaction with either p63 or p73 was observed, showing the high specificity of DARPin C10 for family member p53. **b**, ITC measurements with the control DARPin and the DBDs of all p53 family members. All ITC measurements were performed as technical duplicates with one being shown. The error bars represent the error of the fitting procedure.

https://doi.org/10.1038/s41594-024-01456-7

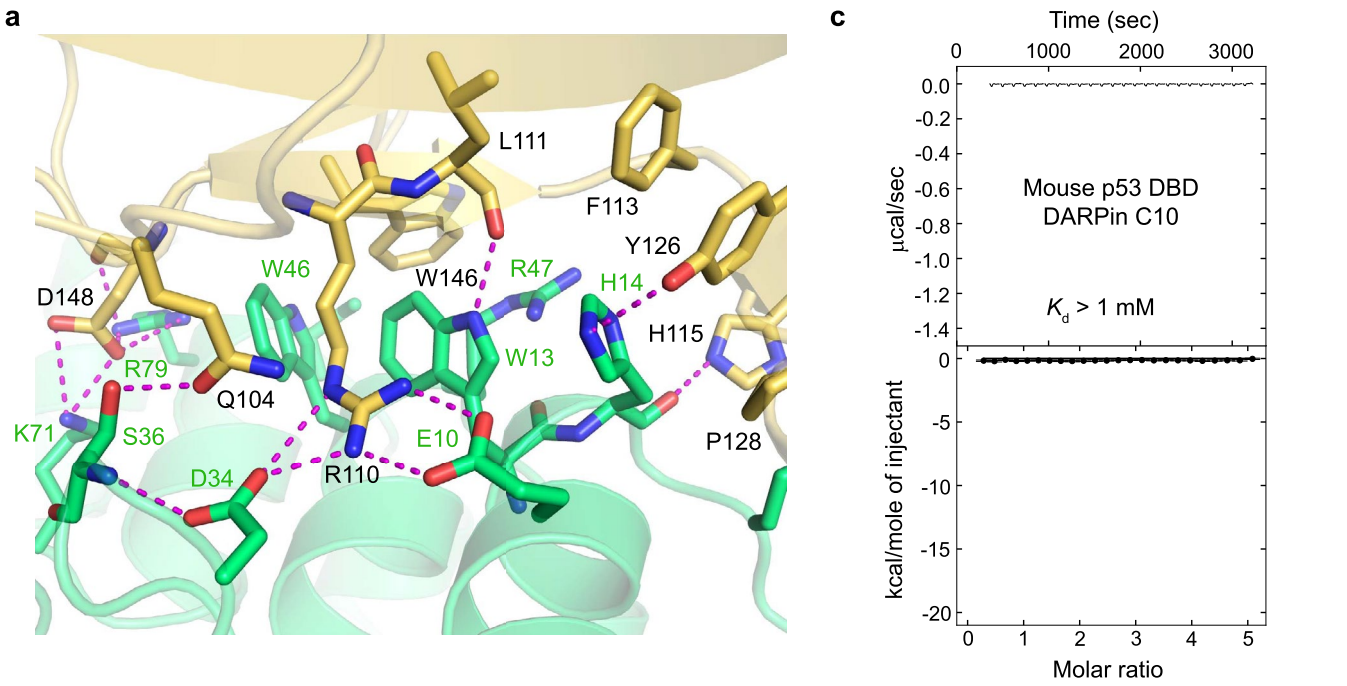

b

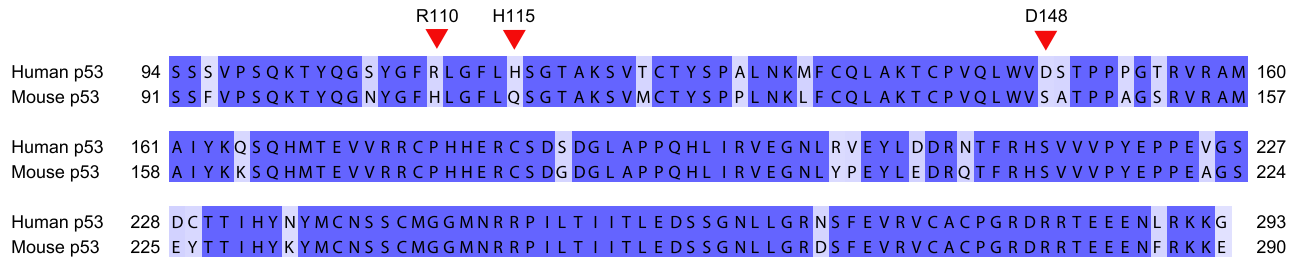

Extended Data Fig. 3 | Binding interface of DARPin C10 and the p53 DBD. a, The structure of the p53 DBD is shown in yellow and that of DARPin C10 in green. Key interacting residues are shown as stick models, and intermolecular salt bridges and hydrogen bonds are highlighted with magenta broken lines. The interface features a hydrophobic patch involving three tryptophan residues, two from the DARPin and one from p53, and two salt-bridge networks via p53 residues Arg110 and Asp148. **b**, Sequence alignment of the human and mouse p53 DBD showing three variations in the DARPin contact surface in the mouse protein (marked with a red triangle), including the crucial salt-bridge forming residues Arg110 and Asp148. Conserved residues are highlighted in blue. (**c**) ITC data for the mouse p53 DBD with DARPin C10. No binding was detected, which can be attributed to variations in the DARPin binding surface in the mouse p53 DBD (see sequence alignment in panel **b**). The ITC measurement shown in this figure was performed at 25 °C as a single experiment.

https://doi.org/10.1038/s41594-024-01456-7

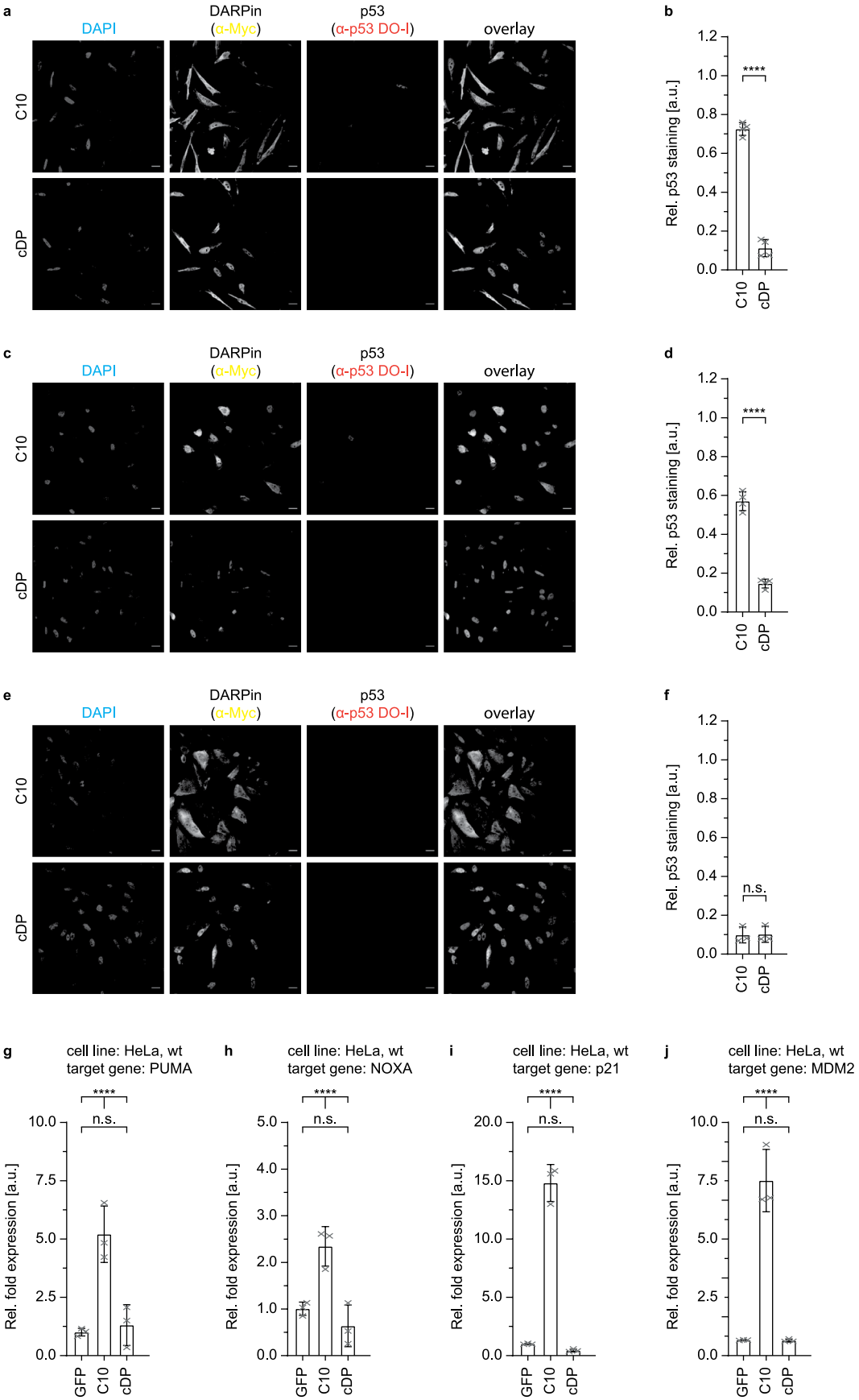

Extended Data Fig. 4 | See next page for caption.

https://doi.org/10.1038/s41594-024-01456-7

Extended Data Fig. 4 | Transfection of cells with mRNA. a, Immunofluorescence staining of HeLa cells transfected with *in vitro* transcribed mRNA encoding DARPin C10 (upper row) or control DARPin (cDP) (lower row). The used mRNA contained the modified nucleotide analogs Ψ-UTP and m^5CTP. The DARPin gene is flanked by the 5'-UTR and 3'-UTR of human beta-globin followed by a 3' poly-A tail of 120 nucleotides. Cells were fixed with formaldehyde and incubated with anti-Myc antibody (Abcam, catalog number ab9106) to detect DARPin expression and α-p53 antibody DO-1 (Santa Cruz Biotechnology) to detect p53 expression, followed by incubation with the secondary antibodies Alexa Fluor 568 anti-rabbit (Life Technologies) and Alexa Fluor 647 anti-mouse (Life Technologies). The scale bar represents 20 µm. **b**, Quantification of the p53 protein level in (**a**). Bar diagrams represent the mean value of four individual images used for the analysis, and error bars depict the corresponding SD. **c**-**f**, Same experiment as in (**a**-**b**) but with SiHa cells (**c**-**d**) or U-2 OS cells (**e**-**f**). **g**-**j**, Transfection of HeLa cells with C10 mRNA results in reactivation of p53 and up-regulation of pro-apoptotic p53 target genes. **g**, RT-qPCR analysis of expression of the PUMA gene in HPV18-positive HeLa cells transfected with mRNA encoding GFP (negative control), C10 or control DARPin (cDP). Total RNA was isolated from the cells and reverse-transcribed into cDNA prior to analysis by quantitative PCR. Gene expression was referenced to the housekeeping gene HPRT-1. **h**-**j**, Same experiment as in (**g**) but with the p53 target genes NOXA (**h**), p21 (**i**), and MDM2 (**j**). In (**d**-**g**), the bar diagrams show the mean values and the error bars the corresponding SD of three biological replicates. An ordinary one-way ANOVA was performed to assess the statistical significance (n.s.: $P > 0.05$, *: $P \leq 0.05$, **: $P \leq 0.01$, ***: $P \leq 0.001$, ****: $P \leq 0.0001$).

https://doi.org/10.1038/s41594-024-01456-7

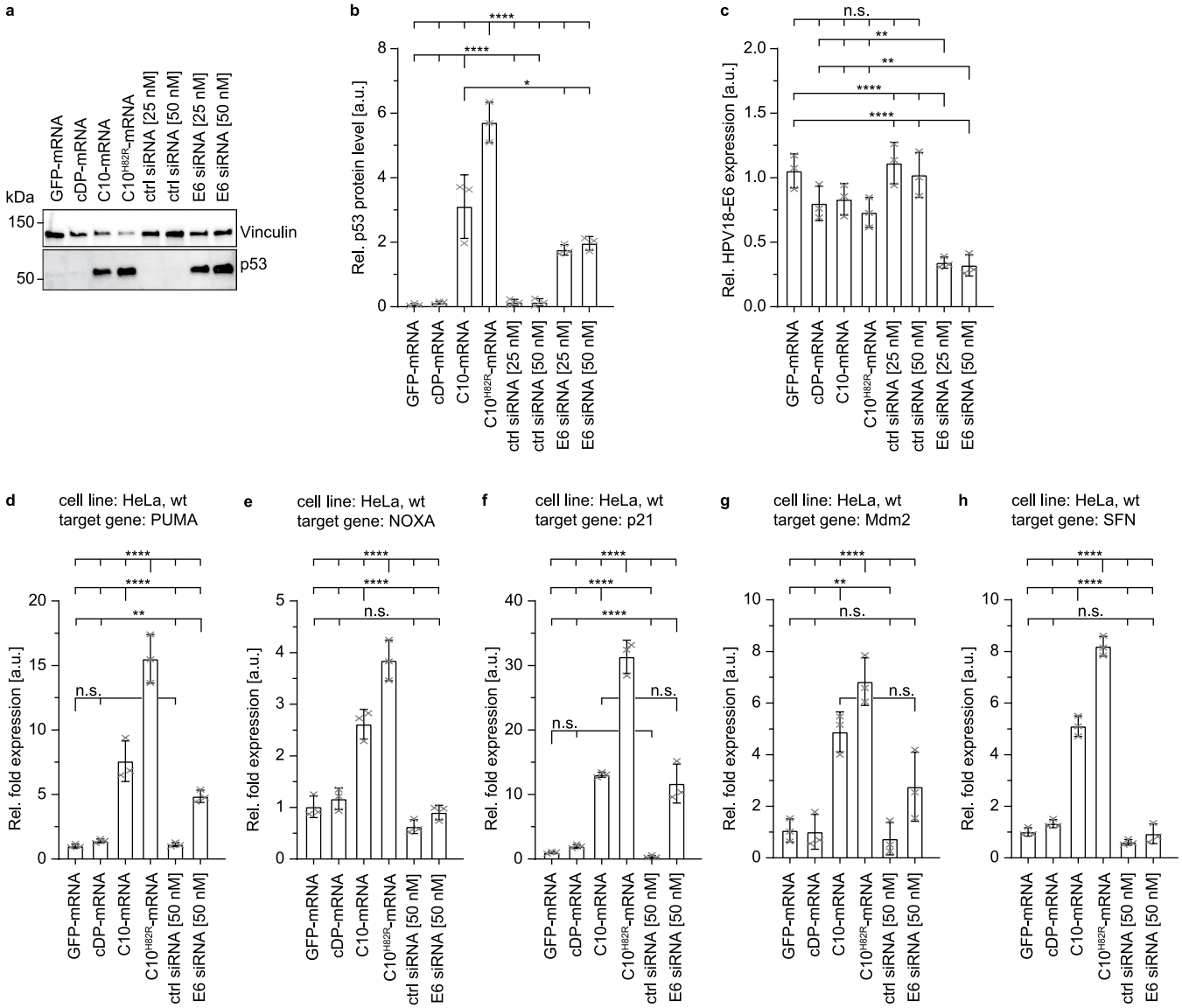

Extended Data Fig. 5 | DARPin-induced reactivation of p53 in HPV18-positive HeLa cells is more efficient than siRNA-mediated knockdown of HPV-E6. a, WB analysis of the p53 protein level in cells transfected with mRNA encoding the respective DARPin or siRNA. The p53 protein level was detected with the α-p53 antibody DO-I (Santa Cruz), and the vinculin level was detected as a loading control. **b**, Quantification of the WB shown in (**a**). The p53 protein level was normalized against the vinculin protein level. **c**, Analysis of the expression level of HPV18-E6 in HeLa cells transfected with mRNA encoding the respective DARPin or the indicated siRNAs by RT-qPCR. Gene expression levels were normalized against the housekeeping gene GAPDH. **d**-**h**, Analysis of the expression of the p53 target genes PUMA (**d**), NOXA (**e**), p21 (**f**), MDM2 (**g**), and SFN (**h**) in HeLa cells transfected with mRNA encoding the respective DARPin or the indicated siRNAs. Gene expression levels were normalized to the housekeeping gene HPRT-1. Bar diagrams display the mean value of three biological replicates, and error bars depict the corresponding standard deviation (SD). An ordinary one-way ANOVA was performed to assess the statistical significance in b-h (n.s.: $P > 0.05$, *: $P \leq 0.05$, **: $P \leq 0.01$, ***: $P \leq 0.001$, ****: $P \leq 0.0001$).

https://doi.org/10.1038/s41594-024-01456-7

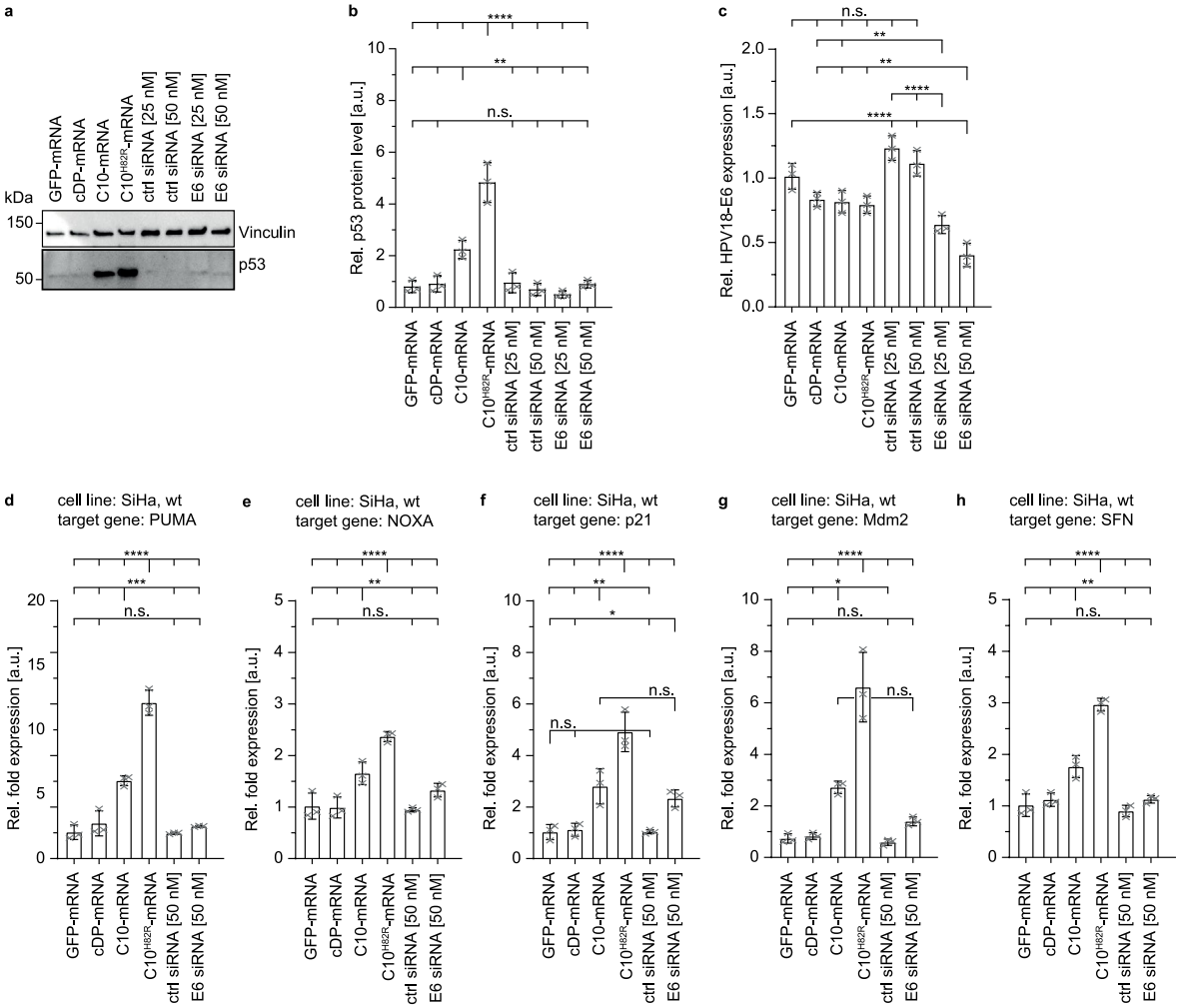

Extended Data Fig. 6 | DARPin-induced reactivation of p53 in HPV16-positive SiHa cells is more efficient than siRNA-mediated knockdown of HPV-E6. a, WB analysis of the p53 protein level in cells transfected with mRNA encoding the respective DARPin or siRNA. The p53 protein level was detected with the α-p53 antibody DO-I (Santa Cruz) and the vinculin level was detected as a loading control. **b**, Quantification of the WB shown in (**a**). The p53 protein level was normalized to the vinculin protein level. **c**, Analysis of the expression level of HPV16-E6 in HeLa cells transfected with mRNA encoding the respective DARPin or the indicated siRNAs by RT-qPCR. Gene expression levels were normalized to the housekeeping gene GAPDH. **d-h**, Analysis of the expression of the p53 target genes PUMA (**d**), NOXA (**e**), p21 (**f**), MDM2 (**g**), and SFN (**h**) in HeLa cells transfected with mRNA encoding the respective DARPin or the indicated siRNAs. Gene expression levels were normalized to the housekeeping gene HPRT-1. Bar diagrams display the mean value of three biological replicates and error bars depict the corresponding standard deviation (SD). An ordinary one-way ANOVA was performed to assess the statistical significance in b-h (n.s.: $P > 0.05$, *: $P \leq 0.05$, **: $P \leq 0.01$, ***: $P \leq 0.001$, ****: $P \leq 0.0001$).

https://doi.org/10.1038/s41594-024-01456-7

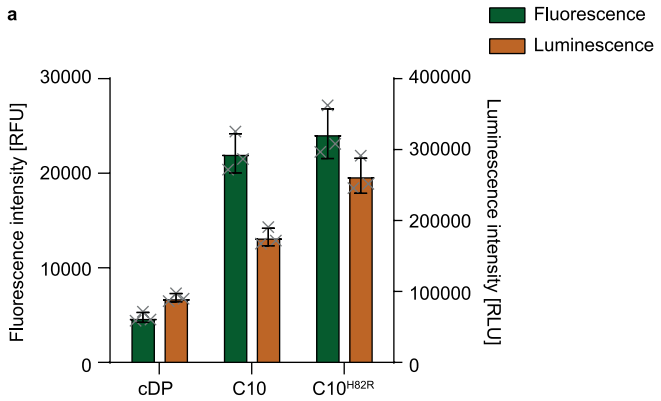

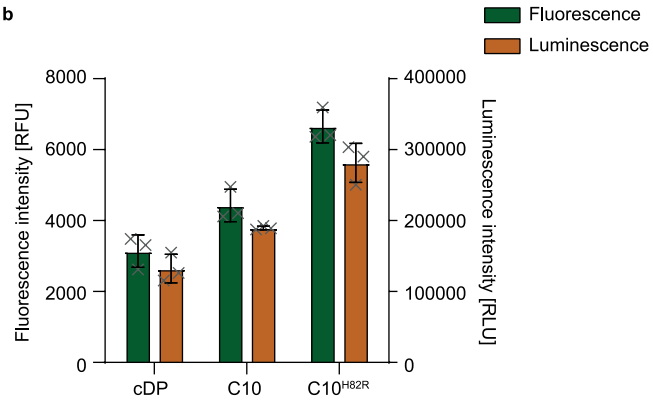

Extended Data Fig. 7 | Expression of DARPin C10 and DARPin C10-H82R induces apoptosis in HPV-positive cells. a, Investigation of cell death induced by DARPin-based reactivation of p53 in HPV18-positive HeLa cells. The Celltox Green Cytoxocity assay (Promega) was performed to detect cell death via fluorescence of a non-membrane-permeable cyanine dye that stains the DNA of dead cells. Apoptosis induction was detected via luminescence using the Caspase Glo 3/7 Assay (Promega). Bar diagrams represent the mean value of three individual biological replicates and error bars the corresponding standard deviation. **b**, Same experiments as in (a) but with HPV16-positive SiHa cells.

nature portfolio

Corresponding author(s): Volker Dötsch

Last updated by author(s): Nov 15, 2024

Reporting Summary

Nature Portfolio wishes to improve the reproducibility of the work that we publish. This form provides structure for consistency and transparency in reporting. For further information on Nature Portfolio policies, see our Editorial Policies and the Editorial Policy Checklist.

Statistics

For all statistical analyses, confirm that the following items are present in the figure legend, table legend, main text, or Methods section.

n/a	Confirmed
☐	☒ The exact sample size (*n*) for each experimental group/condition, given as a discrete number and unit of measurement
☐	☒ A statement on whether measurements were taken from distinct samples or whether the same sample was measured repeatedly
☐	☒ The statistical test(s) used AND whether they are one- or two-sided *Only common tests should be described solely by name; describe more complex techniques in the Methods section.*
☒	☐ A description of all covariates tested
☒	☐ A description of any assumptions or corrections, such as tests of normality and adjustment for multiple comparisons
☐	☒ A full description of the statistical parameters including central tendency (e.g. means) or other basic estimates (e.g. regression coefficient) AND variation (e.g. standard deviation) or associated estimates of uncertainty (e.g. confidence intervals)
☐	☒ For null hypothesis testing, the test statistic (e.g. *F*, *t*, *r*) with confidence intervals, effect sizes, degrees of freedom and *P* value noted *Give P values as exact values whenever suitable.*
☒	☐ For Bayesian analysis, information on the choice of priors and Markov chain Monte Carlo settings
☒	☐ For hierarchical and complex designs, identification of the appropriate level for tests and full reporting of outcomes
☒	☐ Estimates of effect sizes (e.g. Cohen's *d*, Pearson's *r*), indicating how they were calculated

Our web collection on statistics for biologists contains articles on many of the points above.

Software and code

Policy information about availability of computer code

Data collection	Zen 2.3 black edition (Zeiss); MicroCal Control Software (Version 1.40.0, Malvern Instruments Ltd.)
Data analysis	Prism (Version 8.2.1, GraphPad); ImageLab (version 6.1, Bio-Rad); Pymol (version 2.5.2, Schrodinger, Inc., USA); QuantStudio Design and Analysis Software (v1.5.2, Thermo Fisher Scientific); Zen 3.3 blue edition (Zeiss); NITPIC (Version 1.2.7, Keller, S. et al. High-Precision Isothermal Titration Calorimetry with Automated Peak-Shape Analysis. Analytical Chemistry 84, 5066-5073 (2012).), SEDPHAT (Version 12.1b, Houtman, J.C.D. et al. Studying multisite binary and ternary protein interactions by global analysis of isothermal titration calorimetry data in SEDPHAT: Application to adaptor protein complexes in cell signaling. Protein Science 16, 30-42 (2007)); XDS (Version January 10, 2022. BUILT=20220110; Kabsch, W. Xds. Acta Crystallogr D Biol Crystallogr 66, 125-32 (2010).); AIMLESS (Version 0.7.4, used as part of the CCP4 package; Evans, P.R. An introduction to data reduction: space-group determination, scaling and intensity statistics. Acta Crystallographica Section D-Biological Crystallography 67, 282-292 (2011).); CCP4 (Version 7.0.078; Winn, M.D. et al. Overview of the CCP4 suite and current developments. Acta Crystallogr D Biol Crystallogr 67, 235-42 (2011).); PHASER (Version 2.8.3, used as part of the CCP4 package; Mccoy, A.J. et al. Phaser crystallographic software. Journal of Applied Crystallography 40, 658-674 (2007); COOT (Version 0.8.9.2; Emsley, P., Lohkamp, B., Scott, W.G. & Cowtan, K. Features and development of Coot. Acta Crystallographica Section D-Biological Crystallography 66, 486-501 (2010).); PHENIX (Version 1.10.1_2155; Liebschner, D. et al. Macromolecular structure determination using X-rays, neutrons and electrons: recent developments in. Acta Crystallographica Section D-Structural Biology 75, 861-877 (2019)); MolProbity (implemented in PHENIX; Williams, C.J. et al. MolProbity: More and better reference data for improved all-atom structure validation. Protein Sci 27, 293-315 (2018).); PISA server (http://www.ebi.ac.uk/pdbe/prot_int/pistart.html); STAR RNAseq aligner (version 2.7.10a, Dobin, A. et al. STAR: ultrafast universal RNA-seq aligner. Bioinformatics 29, 15-21 (2013).); UMI-tools (version 1.1.2, Smith, T., Heger, A. & Sudbery, I. UMI-tools: modeling sequencing errors in Unique Molecular Identifiers to improve quantification accuracy. Genome Res 27, 491-499 (2017).; DEseq2 (version 1.36.0); matplotlib library (version 3.6.2); GSEA software (version 4.3.2, Subramanian, A. et al. Gene set enrichment analysis: A knowledge-based approach for interpreting genome-wide expression profiles. Proceedings of the National Academy of Sciences of the United States of America 102,

15545-15550 (2005).)67; Molecular Signatures Database (MSigDB, version 7.1); ImageJ 1.54 (Wayne Rasband, NIH, USA); GUSSI (Version 1.4.2, The University of Texas Southwestern Medical Center, USA); ImageLab (version 6.1, Bio-Rad)

For manuscripts utilizing custom algorithms or software that are central to the research but not yet described in published literature, software must be made available to editors and reviewers. We strongly encourage code deposition in a community repository (e.g. GitHub). See the Nature Portfolio guidelines for submitting code & software for further information.

Data

Policy information about availability of data

All manuscripts must include a data availability statement. This statement should provide the following information, where applicable:

- Accession codes, unique identifiers, or web links for publicly available datasets
- A description of any restrictions on data availability
- For clinical datasets or third party data, please ensure that the statement adheres to our policy

The atomic coordinates and structure factors of the p53 DBD complex with DARPin C10 and the DARPin C10-H82R have been deposited in the Protein Data Bank (PDB) under accession code 8RCI and 9ZFB, respectively. RNAseq data were deposited at EBI ArrayExpress, accession number E-MTAB-13602.

Research involving human participants, their data, or biological material

Policy information about studies with human participants or human data. See also policy information about sex, gender (identity/presentation), and sexual orientation and race, ethnicity and racism.

Reporting on sex and gender	not applicable
Reporting on race, ethnicity, or other socially relevant groupings	not applicable
Population characteristics	not applicable
Recruitment	not applicable
Ethics oversight	not applicable

Note that full information on the approval of the study protocol must also be provided in the manuscript.

Field-specific reporting

Please select the one below that is the best fit for your research. If you are not sure, read the appropriate sections before making your selection.

☒ Life sciences ☐ Behavioural & social sciences ☐ Ecological, evolutionary & environmental sciences

For a reference copy of the document with all sections, see nature.com/documents/nr-reporting-summary-flat.pdf

Life sciences study design

All studies must disclose on these points even when the disclosure is negative.

Sample size	typically triplicates were chosen for all pulldown experiments, qPCR analysis etc. Triplicates are the minimum for providing reasonable statistics. Duplicates were used for the measurment of ITC data. The kD values were determined from each experiment separately and the second repeat was only used to confirm that the original measurement was reproducable.
Data exclusions	No data were excluded from analysis.
Replication	Pulldown experiments, p53 degradation assays, transactivation assays, qPCR experiments, si-RNA knockdown assays and cell surival assays were performed in biological triplicates. All experiments were successful. ITC measurements were performed in technical duplicates. Immunofluorescence stainings were performed in biological duplicates. Four to five seperate images were used for quantification of the p53 level.
Randomization	This is not relevant to this study.
Blinding	This is not relevant to this study.

Behavioural & social sciences study design

All studies must disclose on these points even when the disclosure is negative.

Study description	*Briefly describe the study type including whether data are quantitative, qualitative, or mixed-methods (e.g. qualitative cross-sectional, quantitative experimental, mixed-methods case study).*
Research sample	*State the research sample (e.g. Harvard university undergraduates, villagers in rural India) and provide relevant demographic information (e.g. age, sex) and indicate whether the sample is representative. Provide a rationale for the study sample chosen. For studies involving existing datasets, please describe the dataset and source.*
Sampling strategy	*Describe the sampling procedure (e.g. random, snowball, stratified, convenience). Describe the statistical methods that were used to predetermine sample size OR if no sample-size calculation was performed, describe how sample sizes were chosen and provide a rationale for why these sample sizes are sufficient. For qualitative data, please indicate whether data saturation was considered, and what criteria were used to decide that no further sampling was needed.*
Data collection	*Provide details about the data collection procedure, including the instruments or devices used to record the data (e.g. pen and paper, computer, eye tracker, video or audio equipment) whether anyone was present besides the participant(s) and the researcher, and whether the researcher was blind to experimental condition and/or the study hypothesis during data collection.*
Timing	*Indicate the start and stop dates of data collection. If there is a gap between collection periods, state the dates for each sample cohort.*
Data exclusions	*If no data were excluded from the analyses, state so OR if data were excluded, provide the exact number of exclusions and the rationale behind them, indicating whether exclusion criteria were pre-established.*
Non-participation	*State how many participants dropped out/declined participation and the reason(s) given OR provide response rate OR state that no participants dropped out/declined participation.*
Randomization	*If participants were not allocated into experimental groups, state so OR describe how participants were allocated to groups, and if allocation was not random, describe how covariates were controlled.*

Ecological, evolutionary & environmental sciences study design

All studies must disclose on these points even when the disclosure is negative.

Study description	*Briefly describe the study. For quantitative data include treatment factors and interactions, design structure (e.g. factorial, nested, hierarchical), nature and number of experimental units and replicates.*
Research sample	*Describe the research sample (e.g. a group of tagged Passer domesticus, all Stenocereus thurberi within Organ Pipe Cactus National Monument), and provide a rationale for the sample choice. When relevant, describe the organism taxa, source, sex, age range and any manipulations. State what population the sample is meant to represent when applicable. For studies involving existing datasets, describe the data and its source.*
Sampling strategy	*Note the sampling procedure. Describe the statistical methods that were used to predetermine sample size OR if no sample-size calculation was performed, describe how sample sizes were chosen and provide a rationale for why these sample sizes are sufficient.*
Data collection	*Describe the data collection procedure, including who recorded the data and how.*
Timing and spatial scale	*Indicate the start and stop dates of data collection, noting the frequency and periodicity of sampling and providing a rationale for these choices. If there is a gap between collection periods, state the dates for each sample cohort. Specify the spatial scale from which the data are taken*
Data exclusions	*If no data were excluded from the analyses, state so OR if data were excluded, describe the exclusions and the rationale behind them, indicating whether exclusion criteria were pre-established.*
Reproducibility	*Describe the measures taken to verify the reproducibility of experimental findings. For each experiment, note whether any attempts to repeat the experiment failed OR state that all attempts to repeat the experiment were successful.*
Randomization	*Describe how samples/organisms/participants were allocated into groups. If allocation was not random, describe how covariates were controlled. If this is not relevant to your study, explain why.*
Blinding	*Describe the extent of blinding used during data acquisition and analysis. If blinding was not possible, describe why OR explain why blinding was not relevant to your study.*

Did the study involve field work? ☐ Yes ☐ No

Field work, collection and transport

Field conditions	*Describe the study conditions for field work, providing relevant parameters (e.g. temperature, rainfall).*
Location	*State the location of the sampling or experiment, providing relevant parameters (e.g. latitude and longitude, elevation, water depth).*
Access & import/export	*Describe the efforts you have made to access habitats and to collect and import/export your samples in a responsible manner and in compliance with local, national and international laws, noting any permits that were obtained (give the name of the issuing authority, the date of issue, and any identifying information).*
Disturbance	*Describe any disturbance caused by the study and how it was minimized.*

Reporting for specific materials, systems and methods

We require information from authors about some types of materials, experimental systems and methods used in many studies. Here, indicate whether each material, system or method listed is relevant to your study. If you are not sure if a list item applies to your research, read the appropriate section before selecting a response.

Materials & experimental systems

n/a	Involved in the study
☐	☒ Antibodies
☐	☒ Eukaryotic cell lines
☒	☐ Palaeontology and archaeology
☒	☐ Animals and other organisms
☒	☐ Clinical data
☒	☐ Dual use research of concern
☒	☐ Plants

Methods

n/a	Involved in the study
☒	☐ ChIP-seq
☒	☐ Flow cytometry
☒	☐ MRI-based neuroimaging

Antibodies

Antibodies used	The following antibodies and dilutions were used: anti-myc (1:2000, clone 4A6, Millipore), anti-p53 (1:500, DO-I, Santa Cruz Biotechnology), anti-vinculin (1:2000, clone 7F9, Santa Cruz Biotechnology), goat anti-mouse HRP (1:5000, A9917, Sigma Aldrich). rabbit anti-myc (1:500, Abcam ab9106), Alexa Fluor 568 anti-rabbit (1:200, A10042, Life technologies) and Alexa Fluor 647 anti-mouse antibody (1:200, A31571, Life Technologies).
Validation	Antibodies binding to FLAG or myc tags are standard antibodies used in numerous applications. The p53 and vinculin antibodies are also standard antibodies that have been tested in many different labs. Antibodies were validated by overexpression of tagged proteins in H1299 cells and compared to cells not expressing the corresponding tagged proteins.

Eukaryotic cell lines

Policy information about cell lines and Sex and Gender in Research

Cell line source(s)	HeLa cells were obtained from CLS Cell Lines GmbH. SiHa cells were obtained from Biozol. U-2 OS cells were a gift from Prof. Dr. Ivan Đikić (IBCII, Goethe University, Frankfurt am Main), originally obtained from ATCC. T-REx HeLa and T-REx U-2 OS cell lines were obtained from Christian Behrends (Munich Cluster for Systems Neurology (SyNergy), Ludwig-Maximilians-University (LMU), Munich, Germany). H1299 cells were purchased from ATCC.
Authentication	According to companies. HeLa and SiHa cells were obtained directly from the companies. U-2 OS, T-REx HeLa and T-REx U-2 OS cell lines were not authenticated. Cells were passaged a limited number of times before a new batch was used. Cells were monitored by regular visual inspection.
Mycoplasma contamination	The cell lines used in this study were frequently tested negatively for mycoplasma contaminations.
Commonly misidentified lines (See ICLAC register)	No cell line from the list of cross-contaminated or otherwise misidentified cell lines was used.

Palaeontology and Archaeology

Specimen provenance	*Provide provenance information for specimens and describe permits that were obtained for the work (including the name of the issuing authority, the date of issue, and any identifying information). Permits should encompass collection and, where applicable, export.*

Specimen deposition	*Indicate where the specimens have been deposited to permit free access by other researchers.*
Dating methods	*If new dates are provided, describe how they were obtained (e.g. collection, storage, sample pretreatment and measurement), where they were obtained (i.e. lab name), the calibration program and the protocol for quality assurance OR state that no new dates are provided.*

☐ Tick this box to confirm that the raw and calibrated dates are available in the paper or in Supplementary Information.

Ethics oversight	*Identify the organization(s) that approved or provided guidance on the study protocol, OR state that no ethical approval or guidance was required and explain why not.*

Note that full information on the approval of the study protocol must also be provided in the manuscript.

Animals and other research organisms

Policy information about studies involving animals; ARRIVE guidelines recommended for reporting animal research, and Sex and Gender in Research

Laboratory animals	*For laboratory animals, report species, strain and age OR state that the study did not involve laboratory animals.*
Wild animals	*Provide details on animals observed in or captured in the field; report species and age where possible. Describe how animals were caught and transported and what happened to captive animals after the study (if killed, explain why and describe method; if released, say where and when) OR state that the study did not involve wild animals.*
Reporting on sex	*Indicate if findings apply to only one sex; describe whether sex was considered in study design, methods used for assigning sex. Provide data disaggregated for sex where this information has been collected in the source data as appropriate; provide overall numbers in this Reporting Summary. Please state if this information has not been collected. Report sex-based analyses where performed, justify reasons for lack of sex-based analysis.*
Field-collected samples	*For laboratory work with field-collected samples, describe all relevant parameters such as housing, maintenance, temperature, photoperiod and end-of-experiment protocol OR state that the study did not involve samples collected from the field.*
Ethics oversight	*Identify the organization(s) that approved or provided guidance on the study protocol, OR state that no ethical approval or guidance was required and explain why not.*

Note that full information on the approval of the study protocol must also be provided in the manuscript.

Clinical data

Policy information about clinical studies

All manuscripts should comply with the ICMJE guidelines for publication of clinical research and a completed CONSORT checklist must be included with all submissions.

Clinical trial registration	*Provide the trial registration number from ClinicalTrials.gov or an equivalent agency.*
Study protocol	*Note where the full trial protocol can be accessed OR if not available, explain why.*
Data collection	*Describe the settings and locales of data collection, noting the time periods of recruitment and data collection.*
Outcomes	*Describe how you pre-defined primary and secondary outcome measures and how you assessed these measures.*

Dual use research of concern

Policy information about dual use research of concern

Hazards

Could the accidental, deliberate or reckless misuse of agents or technologies generated in the work, or the application of information presented in the manuscript, pose a threat to:

No	Yes	
☒	☐	Public health
☒	☐	National security
☒	☐	Crops and/or livestock
☒	☐	Ecosystems
☒	☐	Any other significant area

Experiments of concern

Does the work involve any of these experiments of concern:

No	Yes	
☒	☐	Demonstrate how to render a vaccine ineffective
☒	☐	Confer resistance to therapeutically useful antibiotics or antiviral agents
☒	☐	Enhance the virulence of a pathogen or render a nonpathogen virulent
☒	☐	Increase transmissibility of a pathogen
☒	☐	Alter the host range of a pathogen
☒	☐	Enable evasion of diagnostic/detection modalities
☒	☐	Enable the weaponization of a biological agent or toxin
☒	☐	Any other potentially harmful combination of experiments and agents

Plants

Seed stocks

Report on the source of all seed stocks or other plant material used. If applicable, state the seed stock centre and catalogue number. If plant specimens were collected from the field, describe the collection location, date and sampling procedures.

Novel plant genotypes

Describe the methods by which all novel plant genotypes were produced. This includes those generated by transgenic approaches, gene editing, chemical/radiation-based mutagenesis and hybridization. For transgenic lines, describe the transformation method, the number of independent lines analyzed and the generation upon which experiments were performed. For gene-edited lines, describe the editor used, the endogenous sequence targeted for editing, the targeting guide RNA sequence (if applicable) and how the editor was applied.

Authentication

Describe any authentication procedures for each seed stock used or novel genotype generated. Describe any experiments used to assess the effect of a mutation and, where applicable, how potential secondary effects (e.g. second site T-DNA insertions, mosiacism, off-target gene editing) were examined.

ChIP-seq

Data deposition

☐ Confirm that both raw and final processed data have been deposited in a public database such as GEO.

☐ Confirm that you have deposited or provided access to graph files (e.g. BED files) for the called peaks.

Data access links
May remain private before publication.

For "Initial submission" or "Revised version" documents, provide reviewer access links. For your "Final submission" document, provide a link to the deposited data.

Files in database submission

Provide a list of all files available in the database submission.

Genome browser session
(e.g. UCSC)

Provide a link to an anonymized genome browser session for "Initial submission" and "Revised version" documents only, to enable peer review. Write "no longer applicable" for "Final submission" documents.

Methodology

Replicates

Describe the experimental replicates, specifying number, type and replicate agreement.

Sequencing depth

Describe the sequencing depth for each experiment, providing the total number of reads, uniquely mapped reads, length of reads and whether they were paired- or single-end.

Antibodies

Describe the antibodies used for the ChIP-seq experiments; as applicable, provide supplier name, catalog number, clone name, and lot number.

Peak calling parameters

Specify the command line program and parameters used for read mapping and peak calling, including the ChIP, control and index files used.

Data quality

Describe the methods used to ensure data quality in full detail, including how many peaks are at FDR 5% and above 5-fold enrichment.

Software

Describe the software used to collect and analyze the ChIP-seq data. For custom code that has been deposited into a community repository, provide accession details.

Flow Cytometry

Plots

Confirm that:

☐ The axis labels state the marker and fluorochrome used (e.g. CD4-FITC).

☐ The axis scales are clearly visible. Include numbers along axes only for bottom left plot of group (a 'group' is an analysis of identical markers).

☐ All plots are contour plots with outliers or pseudocolor plots.

☐ A numerical value for number of cells or percentage (with statistics) is provided.

Methodology

Sample preparation	*Describe the sample preparation, detailing the biological source of the cells and any tissue processing steps used.*
Instrument	*Identify the instrument used for data collection, specifying make and model number.*
Software	*Describe the software used to collect and analyze the flow cytometry data. For custom code that has been deposited into a community repository, provide accession details.*
Cell population abundance	*Describe the abundance of the relevant cell populations within post-sort fractions, providing details on the purity of the samples and how it was determined.*
Gating strategy	*Describe the gating strategy used for all relevant experiments, specifying the preliminary FSC/SSC gates of the starting cell population, indicating where boundaries between "positive" and "negative" staining cell populations are defined.*

☐ Tick this box to confirm that a figure exemplifying the gating strategy is provided in the Supplementary Information.

Magnetic resonance imaging

Experimental design

Design type	*Indicate task or resting state; event-related or block design.*
Design specifications	*Specify the number of blocks, trials or experimental units per session and/or subject, and specify the length of each trial or block (if trials are blocked) and interval between trials.*
Behavioral performance measures	*State number and/or type of variables recorded (e.g. correct button press, response time) and what statistics were used to establish that the subjects were performing the task as expected (e.g. mean, range, and/or standard deviation across subjects).*

Acquisition

Imaging type(s)	*Specify: functional, structural, diffusion, perfusion.*
Field strength	*Specify in Tesla*
Sequence & imaging parameters	*Specify the pulse sequence type (gradient echo, spin echo, etc.), imaging type (EPI, spiral, etc.), field of view, matrix size, slice thickness, orientation and TE/TR/flip angle.*
Area of acquisition	*State whether a whole brain scan was used OR define the area of acquisition, describing how the region was determined.*

Diffusion MRI ☐ Used ☐ Not used

Preprocessing

Preprocessing software	*Provide detail on software version and revision number and on specific parameters (model/functions, brain extraction, segmentation, smoothing kernel size, etc.).*
Normalization	*If data were normalized/standardized, describe the approach(es): specify linear or non-linear and define image types used for transformation OR indicate that data were not normalized and explain rationale for lack of normalization.*
Normalization template	*Describe the template used for normalization/transformation, specifying subject space or group standardized space (e.g. original Talairach, MNI305, ICBM152) OR indicate that the data were not normalized.*
Noise and artifact removal	*Describe your procedure(s) for artifact and structured noise removal, specifying motion parameters, tissue signals and physiological signals (heart rate, respiration).*

Volume censoring

Define your software and/or method and criteria for volume censoring, and state the extent of such censoring.

Statistical modeling & inference

Model type and settings

Specify type (mass univariate, multivariate, RSA, predictive, etc.) and describe essential details of the model at the first and second levels (e.g. fixed, random or mixed effects; drift or auto-correlation).

Effect(s) tested

Define precise effect in terms of the task or stimulus conditions instead of psychological concepts and indicate whether ANOVA or factorial designs were used.

Specify type of analysis: ☐ Whole brain ☐ ROI-based ☐ Both

Statistic type for inference

Specify voxel-wise or cluster-wise and report all relevant parameters for cluster-wise methods.

(See Eklund et al. 2016)

Correction

Describe the type of correction and how it is obtained for multiple comparisons (e.g. FWE, FDR, permutation or Monte Carlo).

Models & analysis

n/a	Involved in the study
☐	☐ Functional and/or effective connectivity
☐	☐ Graph analysis
☐	☐ Multivariate modeling or predictive analysis

Functional and/or effective connectivity

Report the measures of dependence used and the model details (e.g. Pearson correlation, partial correlation, mutual information).

Graph analysis

Report the dependent variable and connectivity measure, specifying weighted graph or binarized graph, subject- or group-level, and the global and/or node summaries used (e.g. clustering coefficient, efficiency, etc.).

Multivariate modeling and predictive analysis

Specify independent variables, features extraction and dimension reduction, model, training and evaluation metrics.